# Distinct phytoplankton groups as key drivers modulating summer $CO_2$ uptake in the northern Antarctic Peninsula

Pedro Senger[1,#,*], Raul Rodrigo Costa[1,2,#], Thiago Monteiro[2,3], Afonso Ferreira[1,4,5], Rodrigo Kerr[2], Tiago Segabinazzi Dotto[6], Eduardo Resende Secchi[7], Carlos Rafael Borges Mendes[1,2,4,5,*]

[1] Laboratório de Fitoplâncton e Microorganismos Marinhos, Instituto de Oceanografia, Universidade Federal do Rio Grande (FURG), Av. Itália, km 8, Rio Grande, RS 96203–900, Brazil

[2] Laboratório de Estudos dos Oceanos e Clima, Instituto de Oceanografia, Universidade Federal do Rio Grande (FURG), Av. Itália, km 8, Rio Grande, RS 96203–900, Brazil

[3] Departamento de Oceanografia, Instituto de Geociências, Universidade Federal da Bahia, R. Barão de Jeremoabo, s/n – Ondina, Salvador, BA 40170-290, Brazil

[4] MARE – Marine and Environmental Sciences Centre/ARNET – Aquatic Research Network, Faculdade de Ciências, Universidade de Lisboa, Campo Grande, 1749–016 Lisboa, Portugal

[5] Departamento de Biologia, Faculdade de Ciências, Universidade de Lisboa, Campo Grande, 1749–016 Lisboa, Portugal

[6] National Oceanography Centre, European Way, Southampton SO14 3ZH, United Kingdom

[7] Laboratório de Ecologia e Conservação da Megafauna Marinha, Instituto de Oceanografia, Universidade Federal do Rio Grande (FURG), Av. Itália, km 8, Rio Grande, RS 96203–900, Brazil

* Corresponding authors. E–mail addresses: pedrosengerbio@furg.br (P. Senger); crmendes@ciencias.ulisboa.pt (C.R.B. Mendes).

[#] Pedro Senger and Raul R. Costa contributed equally to this work (co-first authors)

Running Title: Phytoplankton and $CO_2$ dynamics in NAP.

## Abstract

Recent studies aim to understand the role of northern Antarctic Peninsula (NAP) marine ecosystems in biogeochemical cycles. However, data collection in the NAP remains scarce and generally limited to low-resolution surveys. To address this gap, extensive biological (pigments and microscopy) and physico-chemical data (e.g., temperature, salinity, macronutrients, and inorganic carbon variables) were collected at the sea surface during January 2019. The influence of phytoplankton community composition on sea–air $CO_2$ partial pressure difference ($\Delta pCO_2$) and $CO_2$ flux ($FCO_2$) was assessed across six key subregions: Gerlache and Bransfield Straits, coastal and oceanic Weddell Sea, Drake Passage, and Bellingshausen Sea shelf areas. The Gerlache Strait and coastal Weddell regions acted as $CO_2$ sinks ($\Delta pCO_2 = -14$ µatm and $FCO_2 = -0.37$ mmol $m^{-2}$ $day^{-1}$; –54 µatm and –3.02 mmol $m^{-2}$ $day^{-1}$, respectively), while the oceanic Weddell area was equilibrium ($\Delta pCO_2 \sim 1$ µatm and $FCO_2 = 0.72$ mmol $m^{-2}$ $day^{-1}$). In contrast, the Bransfield Strait, Drake Passage, and Bellingshausen regions acted as $CO_2$ sources, i.e., $\Delta pCO_2$ ($FCO_2$) = 7 µatm (1.16 mmol $m^{-2}$ $day^{-1}$), 39 µatm (4.72 mmol $m^{-2}$ $day^{-1}$), and 8 µatm (1.13 mmol $m^{-2}$ $day^{-1}$), respectively. Across all subregions, $CO_2$ drawdown was driven by non-thermal processes, predominantly biological, with phytoplankton playing a significant role. Subregions dominated by diatoms showed stronger $CO_2$ drawdown compared to those dominated by cryptophytes. Among diatoms, regions dominated by centric rather than pennate diatoms showed higher $CO_2$ uptake, suggesting differences in $CO_2$ uptake between diatom types, although separating their effects is challenging. These results highlight the importance of considering phytoplankton community composition when evaluating sea–air $CO_2$ exchanges in the Southern Ocean.

**Keywords:** Southern Ocean, marine biogeochemistry, diatoms, cryptophytes.

## 1. Introduction

The northern Antarctic Peninsula (NAP) is amongst the most vulnerable areas in the Southern Ocean, experiencing one of the highest atmospheric warming rates on Earth since the 1950s (Kerr et al. 2018a). Rising atmospheric and upper ocean temperatures have been observed in the NAP, leading to changes in glacier retreat and sea ice cycles (Cook et al. 2016). During the austral summer, the meltwater input from sea ice and glacier retreat enhances upper ocean stratification along the NAP, a key factor regulating the distribution and composition of phytoplankton communities (e.g., Mendes et al. 2013, 2018a, 2018b). As a result of long-term ecosystem changes, the dominant diatoms are being increasingly replaced by emerging nanoflagellate groups, such as cryptophytes, in coastal waters of the NAP (Mendes et al. 2023). This shift at the base of the marine food web may have implications for biogeochemical cycles (Monteiro et al. 2023, Santos-Andrade et al. 2023) and energy transfer through higher trophic levels (Ferreira et al. 2020).

The NAP marine system encompasses the Gerlache and Bransfield Straits, the southernmost sector of the Drake Passage and the northwestern Weddell Sea continental shelf (Kerr et al. 2018a). Gerlache Strait, a highly productive coastal region (Costa et al. 2020), is an enclosed area primarily influenced at the surface by water masses from the Bellingshausen Sea (Kerr et al. 2018a). These waters are relatively warm, nutrient-rich, low in oxygen, with high concentrations of dissolved inorganic carbon (DIC) (Hauri et al. 2015). Conversely, deeper layers of Gerlache Strait may be influenced by water masses advected from Weddell Sea (Kerr et al. 2018b), which are comparatively colder, more oxygenated (Dotto et al. 2016, Damini et al. 2023), and poorer in nutrients (Monteiro et al. 2023). Similarly, Bransfield Strait receives advected surface waters from Bellingshausen Sea through the Antarctic Circumpolar Current (Barlett et al. 2018), while also receiving influence of cold waters from the Weddell Sea (Collares et al. 2018). This makes Bransfield Strait extremely dynamic in terms of its oceanographic conditions (Costa et al. 2020, Damini et al. 2025). The northernmost region of the NAP, the Drake Passage, is strongly influenced by warmer waters associated with the Antarctic Circumpolar Current, while the eastern coastal regions influenced by Weddell Sea exhibit colder regimes and occasionally have lower concentrations of nutrients during the summer (Ferreira et al. 2020, Monteiro et al. 2023).

One of the key questions currently driving much of the research in the field of oceanography is understanding the factors that drive $CO_2$ uptake by the oceans and the extent to which these processes may be affected by climate change. In this context, research focusing on phytoplankton is essential, as the variable characteristics of phytoplankton communities influence the sea surface partial pressure of $CO_2$ ($pCO_2^{sw}$) in distinct ways (Carvalho et al. 2022, Kerr et al. 2024). The $pCO_2^{sw}$, as well as derived quantities such as the sea-air $pCO_2$ gradient ($\Delta pCO_2$) and the $CO_2$ flux ($FCO_2$), are modulated by a combination of thermal and non-thermal drivers (Takahashi et al. 2002). The non-thermal factors include water mass mixing (Cao et al. 2020) and biological processes such as photosynthesis, respiration, and calcification (Takahashi et al. 2002, 2009). It is in this latter regard that phytoplankton, as the main primary producer in the oceans, acts as an important driver of $CO_2$ changes. Evidence indicates that phytoplankton species differ in their enzymatic affinities for $CO_2$ uptake, highlighting species-specific adaptations in carbon acquisition strategies (Rost et al. 2003).

In diverse marine and coastal environments, studies have been conducted to explore the relationship between phytoplankton and $pCO_2^{sw}$ changes, in which phytoplankton has been identified as the primary modulator of inorganic carbon dynamics, including in the eastern subarctic Pacific (e.g., Signorini et al. 2001), Indian Ocean (e.g., Sarma et al. 2021), South Atlantic Ocean (e.g., Carvalho et al. 2022, Kerr et al. 2024), and Southern Ocean (e.g., Brown et al. 2019, Costa et al. 2020). Although marine diatoms are traditionally considered the phytoplankton functional group most positively associated with the oceanic $CO_2$ sink (Brown et al. 2019, Costa et al. 2020), recent evidence shows that, despite their abundance in subpolar regions of the Southern Ocean, they may not significantly contribute to deep ocean carbon export, suggesting a potentially lower-than-expected role in long-term carbon sequestration (Williams et al. 2025). Therefore, further studies will be essential to assess the influence of phytoplankton community composition on the ocean carbon sink, especially in climatically sensitive regions such as the Southern Ocean.

In the NAP region – core area of activity for the Brazilian High Latitude Oceanography Group (GOAL; Mata et al. 2018) – numerous independent studies have been conducted focusing on the carbonate system (e.g., Monteiro et al. 2020a, 2020b; Orselli et al. 2022; Santos-Andrade et al. 2023; Kerr et al. 2025; Monteiro et al. 2025) and the dynamics of phytoplankton communities (e.g., Ferreira et al. 2020, Costa et al. 2020, 2021, 2023, Mendes et al. 2023). These efforts have substantially advanced the current knowledge of the region's biogeochemical processes. Nonetheless, integrative approaches are critical to achieving a more comprehensive understanding of the mechanisms driving the carbon cycle in this important region. Thus, the main objective of this work is to investigate the role of phytoplankton communities in the sea surface $p\mathrm{CO_2}$ changes, by integrating information and data that have so far been explored independently.

Certain regions in the NAP, such as Gerlache Strait, have been reported as strong $CO_2$ sinks during summer (Monteiro et al. 2020a, 2020b, Turner et al. 2025). These regions are crucial for biological carbon pump in the Southern Ocean, which contributes disproportionately more for the global carbon sink than other oceans (Henley et al. 2020). However, the limited extent of data collection across the NAP's subregions due to its vast spatial area restricts studies on $CO_2$ dynamics and their main drivers among the different domains of the NAP (Kerr et al. 2025, Monteiro et al. 2025). To fill this gap, we extensively collected phytoplankton (pigments and microscopy analysis) and physico-chemical data (seawater temperature, salinity, macronutrients, and $p\mathrm{CO_2}^{sw}$) at surface waters along the NAP during January 2019. The sampling grid encompasses the southern Drake Passage, Bransfield and Gerlache Straits, Bellingshausen Sea, and offshore and inshore areas of the Weddell Sea. In this study, we evaluate the phytoplankton community composition, biomass accumulation, and physico-chemical conditions to understand how these factors may influence the sea–air $CO_2$ uptake or release behaviour across the NAP subregions.

## 2. Material and methods

### 2.1.1. *Cruise design and sampling collection*

For this study, 98 oceanographic stations (St.) were occupied during the austral summer of 2019 (8–31 January) aboard the Brazilian Navy Research Vessel *Almirante Maximiano*. The sampled region covered a vast area across the NAP, which was divided into six biogeochemical distinct regions (Testa et al. 2021): Bransfield Strait, Drake Passage, Gerlache Strait, Bellingshausen Sea, Continental Weddell, which includes the Antarctic Sound, and the Oceanic Weddell (Fig. 1).

A combined Sea–Bird® CTD (conductivity–temperature–depth instrument) and Carrousel 911+ system equipped with 24 Niskin bottles was used to measure the hydrographic data profiles, such as *in situ* temperature (°C) and salinity. Surface water samples (5 m) were taken in all CTD stations for both dissolved macronutrients and phytoplankton analysis. Cellulose acetate membrane filters were used to filter samples for determination of dissolved inorganic macronutrient concentrations, such as the dissolved inorganic nitrogen (DIN; nitrate + nitrite + ammonium), phosphate and silicic acid. The filtered samples (60 mL) were immediately frozen at −20°C until onshore analysis. For phytoplankton pigments, seawater samples (0.5–2.5 L) were filtered under low vacuum pump through GF/F filters (25 mm diameter and a 0.7 μm pore size) and immediately frozen at –80ºC for the subsequent High-

Performance Liquid Chromatography (HPLC) pigment analysis. Moreover, 250 mL samples were also collected at surface and preserved in amber glass flasks with 2% alkaline Lugol's iodine solution to later evaluate the species composition and cell density of the phytoplankton community using light microscopy.

### 2.1.2. Repeat observations at key stations

To understand how hydrographic properties, phytoplankton community structure, and $p\mathrm{CO_2}^{\mathrm{sw}}$ changed over a short time span along the NAP, three stations were repeatedly sampled over different intervals during January 2019: two in Gerlache Strait (St. G12 and St. G13) and one in Bransfield Strait (St. B44) (see Fig. 1 for stations' locations). Stations G12 and G13 were sampled twice (25 and 30 January 2019), while station B44 was sampled three times (12, 16, and 31 January 2019).

## 2.2. *Physico-chemical parameters*

### 2.2.1. *Mixed Layer Depth and Water Column Stability*

Seawater thermodynamic calculations were performed with the Thermodynamic Equation of Seawater–2010 (TEOS–10). For each CTD cast, the seawater potential density referenced to 0 dbar ($\sigma_\Theta$; kg m$^{-3}$) was determined based on seawater conservative temperature ($\Theta$; °C), absolute salinity ($S_A$; g kg$^{-1}$) and pressure (dbar) data. To examine the water column physical structure, Mixed Layer Depth (MLD; m) and water column stability ($E$, $10^{-6}$ m$^{-1}$) were calculated from 5 m smoothed profiles of $\sigma_\Theta$, due to the high surface variability. MLD was calculated as the depth at which $\sigma_\Theta$ deviates from its 10 m depth value by a threshold of $\Delta\sigma_\Theta = 0.03$ kg m$^{-3}$, according to the criteria established by de Boyer Montégut et al. (2004). $E$ (Eq. 1) was estimated through the Brünt-Väisälä frequency ($N^2$; Eq. 2), where $g$ and $\rho$ refer to the gravity and in situ seawater density, respectively, and *z* refers to vertical variations in the water column.

$$E = \frac{N^2}{g} \; (10^{-6}\, m^{-1}) \qquad (1)$$

$$N^2 = -\frac{g}{\rho}\frac{d\rho}{dz} \; (s^{-2}) \qquad (2)$$

The average *E* between 5 and 150 m (hereafter, upper water column stability) was used to represent the variation of *E* values estimated to each meter within the upper ocean layers (e.g., Costa et al. 2020, 2021).

### 2.2.2. *Meltwater estimation*

To evaluate the influence of meltwater input on the structure of phytoplankton communities, the meltwater percentage (MW%) was estimated as the difference between the salinity measured, on the same station, at surface ($S_{upper}$) and at a greater depth ($S_{deep}$; i.e., at 300 m), as shown in by Eq. 3 (Rivaro et al. 2014). An average sea ice salinity of 6 was assumed (Ackley et al. 1979):

$$\mathrm{MW\%} = \left(1 - \frac{S_{upper} - 6}{S_{deep} - 6} \times 100\right) \qquad (3)$$

This calculation quantifies the total freshwater contribution from melting ice, regardless of whether the source is sea ice or glacial ice.

### 2.2.3. *Macronutrients analysis*

The macronutrients analyses were carried out using a Hach Lange DR5000 UV-Vis spectrometer and measured following the determination methods described by Aminot & Chaussepied (1983), with an accuracy better than ± 3% for DIN and phosphate and ± 5% for silicic acid (Monteiro et al. 2023). Detection limits were 0.11 µM for DIN, 0,10 µM for phosphate, and 0.5 µM for silicic acid. The reproducibility of the analyses, based on duplicates of the samples, was 1.0% for DIN, 0.7% for phosphate, and 1.0% for silicic acid. In addition, in the form of reactive Si, silicic acid measurements were corrected for sea salt interference, while orthophosphate was quantified through its reaction with ammonium molybdate, with absorption reading at 885 nm (Grasshoff et al. 2009). No certified nutrient reference material was used, in common with other datasets along the NAP and adjacent regions (e.g., Monteiro et al. 2023). For more details on the acquisition and analysis of the macronutrients, see Monteiro et al. (2023).

### **2.2.4.** ***$CO_2$ partial pressure and sea-air $CO_2$ fluxes***

The $pCO_2^{sw}$ was measured continuously at surface (5 m) along the ship tracks, through the continuous equilibration of seawater with a closed loop of air and an integrated non–dispersive infrared $CO_2$ detector (LI–COR® LI–7000). The $CO_2$ mole fraction in the equilibrated gas was compared with $CO_2$–free high–purity nitrogen and four master $CO_2$ standards obtained from White Martins® in compressed air that were used as primary standards. The nominal mole fractions of these standards were 250.9, 381.7 and 472.3 and 599.5 ppm. The $pCO_2^{sw}$ was calculated from the mole fraction corrected for the atmospheric pressure and the partial pressure of saturated water vapor, in accordance with Weiss & Price (1980). The precision and the accuracy of the $pCO_2^{sw}$ measurements were determined to be within ± 0.3 µatm and ± 2.0 µatm, respectively. Here, we used the $pCO_2^{sw}$ measured during the

CTD casts. For more details on the acquisition and analysis of the $pCO_2^{sw}$, see Kerr et al. (2025).

We evaluated the sea–air $CO_2$ difference ($\Delta pCO_2$) based on the difference between $pCO_2^{sw}$ and atmospheric $pCO_2$ ($pCO_2^{air}$). Additionally, the net sea-air $CO_2$ flux ($FCO_2$) was calculated by Equation 4:

$$FCO_2 = K_t K_s \Delta pCO_2 \qquad (4)$$

where $K_t$ is the gas transfer velocity as a function of wind speed, following Wanninkhof (2014); and $K_s$ is the $CO_2$ solubility coefficient, which was calculated as a function of both temperature and salinity (Weiss 1974). We used the underway $pCO_2^{air}$ measured by the $pCO_2$ system and wind speed at 10 m above sea level obtained from January 2019 average wind speed atmospheric reanalysis ERA5 (https://cds.climate.copernicus.eu/), with a spatial resolution of 0.25° (Hersbach et al. 2020). See Kerr et al. (2025) for more details on these approaches.

It is important to highlight that, in this study, $\Delta pCO_2$ is a more appropriate variable than $FCO_2$ for assessing the influence of primary producers on $pCO_2$ drawdown, as it avoids the inclusion of additional parameters (e.g., wind speed) in the calculation. However, reporting both $\Delta pCO_2$ and $FCO_2$ allows us to link the biological drivers to actual sea–air $CO_2$ fluxes, providing a more comprehensive view of $CO_2$ dynamics in the study area. $\Delta pCO_2$ is directly proportional to $FCO_2$, meaning that positive values of both $\Delta pCO_2$ and $FCO_2$ indicate $CO_2$ release from the sea surface to the atmosphere, while negative values reflect $CO_2$ uptake, typically associated with phytoplankton growth during the austral summer (e.g., Brown et al. 2019; Costa et al. 2020; Orselli et al. 2022).

### 2.2.5. *Thermal and non–thermal effect on $pCO_2^{sw}$*

To assess the thermal ($pCO_2^{T}$) and non-thermal ($pCO_2^{nonT}$) effect on $pCO_2^{sw}$ changes, we used the approach of Takahashi et al. (2002), following Eqs. 5 and 6:

$$pCO_2^{nonT} = pCO_2^{obs} \times \exp [0.0423 \times (T_{avg} - T_{obs})] \qquad (5)$$

$$pCO_2^{T} = pCO_2^{avg} \times \exp [0.0423 \times (T_{obs} - T_{avg})], \qquad (6)$$

where $pCO_2^{obs}$ and $T_{obs}$ are *in situ* $pCO_2^{sw}$ and Θ, respectively, while $T_{avg}$ and $pCO_2^{avg}$ are averages of Θ (0.81°C) and $pCO_2^{sw}$ (404 µatm), respectively. Changes in $pCO_2^{nonT}$ represent primarily changes in the total $CO_2$ concentration, which include processes other than changes driven by temperature ($pCO_2^{T}$), such as biological activity, sea ice growth or sea ice melting, sea–air $CO_2$ exchanges, and advection or upwelling of water masses.

The thermal (T) and non-thermal (nonT) effects of $pCO_2^{sw}$ changes were represented by the amplitude of $pCO_2^{T}$ and $pCO_2^{nonT}$ in each subregion, according to Eqs. 7 and 8, respectively.

$$T\ effect = (pCO_2^{T})_{max} - (pCO_2^{T})_{min} \qquad (7)$$

$$NonT\ effect = (pCO_2^{nonT})_{max} - (pCO_2^{nonT})_{min} \qquad (8)$$

The relative importance of T and nonT effects on $pCO_2^{sw}$ is expressed by the T:nonT ratio. The ratio is greater than 1 when the effect of temperature on $pCO_2^{sw}$ exceeds the non-thermal effect, whereas when the non-thermal effect exceeds the temperature effect, it is less than 1. As highlighted above, besides thermal effects, non-thermal processes modulating $pCO_2^{sw}$ are assumed here to be predominantly driven by biological activity and, where relevant, by sea ice processes, reflecting the characteristics of the study area.

### 2.2.6. *Total alkalinity and dissolved inorganic carbon*

Total alkalinity (Alk) was estimated from sea surface salinity, using the equation by Monteiro et al. (2020a) (Alk = 36.72 × salinity + 1052). Uncertainty in estimating Alk by this approach is expected to be ± 4.4 µmol kg$^{-1}$ (Monteiro et al. 2020a). We tested CANYON-B neural network approach (Bittig et al. 2018) and some regional Alk algorithms (i.e., Hauri et al. 2015; Monteiro et al. 2020a, b) to assess the estimated Alk performed here, with the largest average absolute difference being 13 ± 9 µmol kg$^{-1}$ as observed by Orselli et al. (2022). These absolute differences are smaller than the spatial variability observed in the NAP subregions analysed here (2283–2319 µmol kg$^{-1}$) and are comparable to the uncertainties in Alk estimates from CANYON-B (11 µmol kg$^{-1}$), Hauri et al. (2015) (15 µmol kg$^{-1}$) and Monteiro et al. (2020b) (16.8 µmol kg$^{-1}$). For more details on the use of reconstructed Alk, see Monteiro et al. (2025).

The dissolved inorganic carbon (DIC) was calculated from Alk and $p\mathrm{CO_2}^{sw}$, derived from the thermodynamic equilibrium of the carbonate system in CO2SYS v2.1 program (Pierrot et al. 2006) using the same equilibrium constants described in Monteiro et al. (2020a, b) and widely used throughout the NAP (e.g., Orselli et al. 2022, Santos-Andrade et al. 2023, Monteiro et al. 2025). The propagated uncertainty in the DIC calculation was estimated as 11 ± 2 µmol kg$^{-1}$ using the CO2SYS error tool by Orr et al. (2018). Despite the uncertainty (~11 µmol kg$^{-1}$), the estimates are considered robust for assessing spatial patterns in DIC, as this variability largely exceeds the propagated error (Monteiro et al. 2025). The ratio between Alk and DIC can be used to diagnose the physical-biological processes influencing them and therefore the carbonate–$CO_2$ system, as each process alters Alk and DIC with a certain ratio (Zeebe & Wolf-Gladrow 2001, Yin et al. 2024). Such ΔAlk:ΔDIC ratios are as follows: 0.86:1 for ice–melt/ice–growth (Monteiro et al. 2020a), 2:1 for calcification/dissolution, −0.14:1 for photosynthesis/respiration, whereas only DIC is altered in sea–air $CO_2$ release/uptake processes (e.g., Zeebe & Wolf-Gladrow 2001). To eliminate the influence of sea ice melt dilution, Alk and DIC were normalised by the average sea surface salinity of 34.1 g kg$^{-1}$ obtained in the study region, using non-zero freshwater endmembers (Alk$^{S=6}$; DIC$^{S=6}$; Friis et al. 2003). The endmembers used were Alk$^{S=6}$ = 451 μmol kg$^{-1}$ and DIC$^{S=6}$ = 480 μmol kg$^{-1}$, proposed by Rysgaard et al. (2011), who measured Alk and DIC concentrations in brine channels of sea ice (salinity = 6) and surrounding waters in Antarctica.

## 2.3. *Biological parameters*

### 2.3.1. *HPLC analysis*

Following the procedures described in Mendes et al. (2007), the filters were placed in a screw–cap centrifuge tube with 3 mL of 95% cold–buffered methanol (2% ammonium acetate) containing 0.05 mg L$^{-1}$ trans–β–apo–8'–carotenal (Fluka) as internal standard. Samples were sonicated for 5 minutes in an ice–water bath, placed at –20°C for 1 hour, and then centrifuged at 1100g for 5 minutes at 3°C. The supernatants were filtered through Fluoropore PTFE membrane filters (0.2 μm pore size) to separate the extract from remains of filter and cell debris. Immediately prior to injection, 1000 μL of sample was mixed with 400 μL of Milli–Q water in 2.0 mL amber glass sample vials, which then were placed in the HPLC cooling rack (4°C). The pigment extracts were analysed using a Shimadzu HPLC constituted by a solvent distributor module (LC–20AD) with control system (CBM–20A), a photodiode detector (SPD–M20A) and a fluorescence detector (RF–10AXL). The chromatographic separation of the pigments was performed using a monomeric C8 column (SunFire; 15 cm long; 4.6 mm in diameter; 3.5 μm particle size) at a constant temperature of 25°C. The mobile phase (solvent) and respective gradient followed the method developed by Zapata et al. (2000), discussed and optimised by Mendes et al. (2007), with a flow rate of 1 mL min$^{-1}$, injection volume of 100 μL, and 40 minutes runs.

All pigments, including chlorophyll-*a* (chl-*a*), were identified from both absorbance spectra and retention times, and the concentrations were calculated from the signals in the photodiode array detector in comparison with commercial standards obtained from DHI (Institute for Water and Environment, Denmark). The peaks were integrated using LC–Solution software v5.73, and all peak integrations were manually checked and corrected when necessary. A quality assurance (QA) threshold procedure, through application of quantification limit (LOQ) and detection limit (LOD), was applied to the pigment data, as described by Canuti et al. (2022). The LOQ and LOD procedures were performed according to Mendes et al. (2007). The pigment concentrations were normalised in respect to the internal standard to correct for losses and volume changes (Canuti et al. 2022).

Three types of chl-*a* degradation products: chlorophyllide-*a*, pheophytin-*a*, and pheophorbide-*a* were identified and quantified by HPLC analysis. Pheophytin-*a* and chlorophyllide-*a* are derived from chl-*a* by losing the Mg atom and the phytol chain, respectively, while the loss of both chl-*a* structures generates the pheophorbide-*a* (Shaman & Lorenzen 1975). The loss of Mg atom is associated with zooplankton gut-related acid exposure, whereas phytol chain can be removed by light action and/or cell stress (Moreth & Yentsch 1970). Pheopigments-*a* (pheophytin-*a* plus pheophorbide-*a*) have long been found in the faecal material of zooplankton (Jeffrey et al. 1974). Therefore, we used the sum of the pheophytin-*a* and pheophorbide-*a* as a proxy of grazing pressure, and chlorophyllide-*a* as a proxy of senescence of phytoplankton cells, similarly to what has already been used in several other studies on phytoplankton ecology in the NAP region (e.g., Mendes et al. 2012, Costa et al. 2020, 2021, 2023, Mendes et al. 2023). These two indices were divided by the total of degradation products plus chl-*a* (sum of chl-*a*, chlorophyllide-*a*, pheophytin-*a*, and pheophorbide-*a*), and represented as a percentage (Costa et al. 2023).

### 2.3.2. *CHEMTAX analysis*

The absolute (mg $m^{-3}$ chl-*a*) and relative (%) contribution of phytoplankton chemotaxonomic groups to the total chl-*a* were estimated via CHEMTAX software v1.95 (Mackey et al. 1996). CHEMTAX uses a factor analysis and steepest descent algorithm to best fit the data onto an initial matrix of pigment ratios (i.e., the ratios between the accessory pigments and chl-*a*). The procedures and calculations are fully described in Mackey et al. (1996). Although chl-*a* concentration is not an absolute measure of algal biomass, such as carbon, it is widely accepted as a proxy for biomass since it is common to all autotrophic phytoplankton species (Jeffrey et al. 1974, Huot et al. 2007). Therefore, in this way, the term chl-*a* refers to either absolute biomass or relative biomass attributed to the corresponding chemotaxonomic groups (Mendes et al. 2012, 2013, 2018a, 2018b, Costa et al. 2020). Based on the identified diagnostic pigments and previous experience in the region (e.g., Mendes et al. 2012, 2013, 2018a, 2018b, 2023, Costa et al. 2020, 2021, 2023), seven algal groups were chosen for CHEMTAX analysis: diatoms type–A, diatoms type–B, dinoflagellates type–A, dinoflagellates type–B, cryptophytes, haptophytes type 8 (*Phaeocystis antarctica*) and green flagellates. After applying CHEMTAX analysis, the two types of diatoms and dinoflagellates were grouped as a same chemotaxonomic group: the diatoms (sum of diatoms type–A and diatoms type–B) and the dinoflagellates (sum of dinoflagellates type–A and dinoflagellates type–B), respectively. The biomarker pigments and their respective phytoplankton functional groups are shown in the Supplementary Material Table S1.

The whole pigment dataset was separated according to the six subregions considered in this study: Bransfield Strait, Drake Passage, Gerlache Strait, Bellingshausen Sea, Continental Weddell, and Oceanic Weddell. They were separately analysed by CHEMTAX to allow for variation in pigment: chl-*a* ratios (Mackey et al. 1996). This procedure assured a homogeneity of the pigment: chl-*a* ratios, providing some compensation for changes in these ratios. For optimization of the input matrix, a series of 60 pigment ratio matrices were generated by multiplying each ratio from the initial matrix by a random function as described in Wright et al. (2009). The average of the best six (10%) output matrices, i.e., with the lowest residual or mean square root error (RMS), was taken as the optimised result. The results of phytoplankton chemotaxonomic groups derived from the CHEMTAX were quality-controlled by microscopic analysis.

### 2.3.3. *Microscopic analysis*

Settling chambers (2-, 10-, or 50-mL settling volume) were inspected on an Axiovert 135 ZEISS inverted light microscopy (Utermöhl 1958, Sournia 1978) at 100×, 200×, and 400× magnification, following previous literature (e.g., Scott & Marchant 2005). The microscopic analyses were used in this study to validate the HPLC/CHEMTAX results, and to quantitatively characterise the diatom composition in the region. Regarding to diatoms, since this functional group can exhibit a large diversity of shapes, we use microscopy analysis to quantify the density (cells $L^{-1}$) of diatom genera. We grouped the diatom genera in centric or pennate diatoms (Supplementary Material Table S2).

## 2.4. *Statistical analysis*

Canonical correspondence analysis (CCA; Ter Braak & Prentice 1988) is a multivariate method that relates species/groups abundance to environmental variables, extracting gradients that explain variation in community composition. Here, using CANOCO for Windows v4.5, a CCA was performed to identify the main patterns of the phytoplankton community structure in respect to environmental variables. We considered only surface data (5 m) in this analysis. The biotic data were represented by the relative contribution of phytoplankton groups (%), derived from the CHEMTAX analysis. Explanatory variables included: temperature, salinity, meltwater percent, DIN, phosphate, silicic acid, upper water column stability, MLD, grazing and senescence indexes. Monte-Carlo tests were run on 499 permutations under a reduced model to evaluate the significance of the CCA analysis (*p*-value = 0.002). Furthermore, linear regression analyses were used to evaluate the relationship between chl-*a* and $\Delta p\mathrm{CO_2}$ over the NAP subregions (see Table S3 in the Supplementary Material). This latter approach was chosen as a first-order exploratory method, supported by previous studies that have reported significant linear relationships between phytoplankton biomass and $CO_2$ dynamics in marine and coastal systems (e.g., Yang et al. 2016, Lapierre et al. 2017), despite the recognized complexity of the underlying biogeochemical processes.

## 3. Results

### 3.1. Environmental and biological parameters

The spatial distribution of the NAP subregions is presented in Figure 2a. Average surface temperature was high in the Gerlache Strait (1.50°C) and Bellingshausen Sea (1.44°C) subregions, while low average values were observed in the Continental Weddell (–0.32°C) and Oceanic Weddell (–0.23°C). Intermediate average values were found in the Drake Passage (0.68°C) and Bransfield Strait (0.8°C) subregions (Fig. 2b). Sea surface salinity showed low average values in the Oceanic Weddell (33.98), Gerlache Strait (33.83), and Bellingshausen Sea (33.86), while high average values were observed in the Continental Weddell (34.36), Drake Passage (34.35), and Bellingshausen Sea (34.28) subregions (Fig. 2c). Shallow MLD was recorded on average in the Gerlache Strait (17.6 m), Oceanic Weddell (22 m), and Continental Weddell (25.1 m), while Bransfield Strait (40.7 m) and Bellingshausen Sea (31.8 m) subregions showed relatively deep MLD. The deepest average MLD was observed in the Drake Passage subregion (77.2 m). There was a clear association between average values of upper water column stability and meltwater percent. High average values of stability and meltwater percent were observed in the Gerlache Strait ($1.08 \times 10^{-6}$ m$^{-1}$ and 2.28%, respectively) and Bellingshausen Sea ($0.75 \times 10^{-6}$ m$^{-1}$ and 2.66%), while low average values were found in the Drake Passage ($0.08 \times 10^{-6}$ m$^{-1}$ and 0.7%) and Bransfield Strait ($0.16 \times 10^{-6}$ m$^{-1}$ and 0.8%) subregions. Oceanic Weddell ($0.36 \times 10^{-6}$ m$^{-1}$ and 2.02%) and Continental Weddell ($0.68 \times 10^{-6}$ m$^{-1}$ and 0.42%) showed intermediate average values (Fig. 2c).

The Gerlache Strait subregion had the highest average concentration of chl-*a* (2.84 mg m$^{-3}$). Although a localized bloom (~11.5 mg m$^{-3}$ of chl-*a*) was recorded in the Bransfield Strait, the average for this subregion was 1.8 mg m$^{-3}$. In the most offshore portion of the Weddell Sea, low average chl-*a* was observed (0.25 mg m$^{-3}$), while its more coastal waters (Continental Weddell subregion) exhibited an average chl-*a* concentration above 2.0 mg m$^{-3}$. The Drake Passage subregion had an average chl-*a* of 1.23 mg m$^{-3}$, slightly lower than the Bellingshausen Sea subregion (Fig. 2d and Supplementary Material Table S3).

In the study period, diatoms (Fig. 2e) and cryptophytes (Fig. 2f) dominated the phytoplankton community composition along the NAP. Such functional groups were spatially segregated (Fig. 2e,f). Diatoms represented more than 50% of the phytoplankton community composition in the most stations of the Bransfield Strait, Drake Passage, Bellingshausen Sea, Continental Weddell, and Oceanic Weddell, while cryptophytes showed higher proportions (usually >60% to the total biomass) in the Gerlache Strait (Fig. 2e,f). Other phytoplankton groups (i.e., dinoflagellates, *P. antarctica*, and green flagellates) did not exhibit proportions higher than 25% (Fig. 2g-i, respectively). Importantly, the surface macronutrient concentrations were high across the study area, despite varying between subregions. We did not observe concentrations of macronutrients that would be expected to limit phytoplankton growth since DIN, silicic acid and phosphate were all found in concentrations higher than 15 μM, 40 μM and 0.7 μM, respectively (Fig. 2j-l).

### 3.2. Environmental and biological relationships

Significant and distinct associations were observed between phytoplankton community composition and environmental variables across the different subregions (Fig. 3). Ten selected variables significantly contributed to the spatial distribution of phytoplankton groups. The CCA explained 92.5% of the variance associated with the phytoplankton–environmental relationship, with the first canonical axis explaining 86.1% of the variance. The Gerlache Strait subregion was associated with higher temperatures and concentrations of silicic acid and phosphate. Higher upper water column stability, coupled with meltwater percent along the first axis, was also associated with stations in the Gerlache Strait subregion, where higher proportions of cryptophytes were found (Fig. 3). On the other hand, the stations of the Bransfield Strait were positively associated with deeper MLD and higher values of surface salinity, grazing index, and DIN. For the first axis, high proportions of diatoms were related to stations of all subregions, except for the Gerlache Strait, where cryptophytes dominated. There were some similarities between the Drake Passage and Bransfield Strait, especially regarding the MLD. The Drake Passage subregion was also associated with higher meltwater percent. The Bellingshausen Sea subregion was in turn associated with higher temperatures, senescence index, upper water column stability and meltwater percent. Both continental and oceanic Weddell for the first axis demonstrated a negative relationship with temperature and concentrations of silicic acid and phosphate. The Continental was associated with high values of grazing index, while Oceanic Weddell was associated with high values of senescence index.

### 3.3. Sea–air $CO_2$ differences and T:nonT ratios

The highest $\Delta p\mathrm{CO_2}$ was observed in the Drake Passage (39 ± 33 µatm), accompanied by an $\mathrm{FCO_2}$ value indicating $CO_2$ outgassing (4.72 ± 3.79 mmol $m^{-2}$ $day^{-1}$). The Bransfield Strait and Bellingshausen Sea showed average $\Delta p\mathrm{CO_2}$ values of approximately 10 µatm, with corresponding $FCO_2$ fluxes of 1.16 ± 2.68 mmol $m^{-2}$ $day^{-1}$ and 1.13 ± 1.01 mmol $m^{-2}$ $day^{-1}$, respectively. Both subregions also showed similar $pCO_2^{nonT}$ of 415 µatm (see Fig. 4). In the Oceanic Weddell subregion, the average $\Delta pCO_2$ was approximately 1 µatm, indicating near-equilibrium conditions for $CO_2$ exchange, with an associated $FCO_2$ of 0.72 ± 0.56 mmol $m^{-2}$ $day^{-1}$. Conversely, the Gerlache Strait and Continental Weddell subregions exhibited negative average $\Delta pCO_2$ values of –14 µatm and –54 µatm, corresponding to $CO_2$ sinks of –0.37 ± 1.61 mmol $m^{-2}$ $day^{-1}$ and –3.02 ± 3.88 mmol $m^{-2}$ $day^{-1}$, respectively (Fig. 4 and Supplementary Material Tables S3 and S4). The non–thermal effects on $pCO_2^{sw}$ were assessed through the T:nonT ratios, which were on average lower than 0.5 over all subregions. The Continental Weddell was the subregion with the greatest non–thermal effect on $pCO_2^{sw}$ changes, whilst Oceanic Weddell was the one with the greatest thermal effect (see Table S4 in the Supplementary Material for all T:nonT ratio values). In addition, we used Alk and DIC data to assess which non-thermal process is modulating $pCO_2^{sw}$ changes in each subregion (Fig. 5). All sub-regions, except Oceanic Weddell, exhibited negative ΔAlk:ΔDIC around –0.03, suggesting that changes in the carbonate system are likely driven by photosynthesis/respiration processes. In contrast, that offshore part of Weddell was the only subregion with a positive ΔAlk:ΔDIC ratio (0.15), indicating that sea–air $CO_2$ exchanges, associated with sea-ice melting/growth, were key processes controlling changes in the carbonate system and, consequently, $pCO_2^{sw}$ (Fig. 5).

### 3.4. $\Delta pCO_2$ vs Chlorophyll-*a*

We used the slope of the linear regression between $\Delta pCO_2$ and surface chl-*a* values over the subregions to indicate the correlation between the sea–air $CO_2$ gradient and the phytoplankton biomass (Supplementary Material Table S3). The strongest negative relationship was observed in the Continental Weddell subregion (–66 µatm per mg chl-*a* $m^{-3}$), while the Oceanic Weddell showed an approximately neutral $\Delta p\mathrm{CO_2}$ response per unit chlorophyll-*a* (0.5 µatm per mg chl-*a* $\mathrm{m^{-3}}$). Notably, strong $\mathrm{CO_2}$ undersaturation was also associated with high chl-*a* concentration in Drake Passage (–58 µatm per mg chl-*a* $\mathrm{m^{-3}}$). The Bransfield and Gerlache Straits and Bellingshausen Sea subregions showed a similar $\mathrm{CO_2}$ undersaturation association pattern with chl-*a* concentration (–12, –17, and –18 µatm per mg chl-*a* $\mathrm{m^{-3}}$, respectively). The same pattern was observed when chl-*a* was correlated with DIC instead of $\Delta p\mathrm{CO_2}$ (see Table S5 in the Supplementary Material), with the Continental Weddell and Drake Passage subregions showing higher DIC drawdown rates per mg chl-*a* $\mathrm{m^{-3}}$ (–31 and –30, respectively).

### 3.5. Diatom taxa composition

Centric diatoms showed high abundances in the Bransfield Strait and Continental Weddell subregions, with *Thalassiosira* spp. averaging $5.8 \times 10^3$ and $4.2 \times 10^3$ cells $\mathrm{L^{-1}}$, and *Chaetoceros* sp. averaging $0.7 \times 10^3$ and $14.5 \times 10^3$ cells $\mathrm{L^{-1}}$, respectively. Pennate diatoms were mainly represented by *Fragilariopsis* sp. and *Pseudo-nitzschia* sp., which showed the highest average values in the Gerlache Strait and Bellingshausen Sea, respectively. In addition, *Pseudo-nitzschia* sp. also exhibited high average densities in the Bransfield Strait, Drake Passage, and Gerlache Strait subregions (Table S2 in the Supplementary Material).

### 3.6. Short-interval station resampling

#### 3.6.1. Bransfield Strait

Changes in upper ocean stability at St. B44 were observed between the sampling periods, resulting in shifts of phytoplankton community composition (Fig. 6a). During the first sampling at B44 on 12 January 2019, the upper ocean stability was low ($0.13 \times 10^{-7}$ $\mathrm{m^{-1}}$), with MLD exceeding 20 m. Under such conditions, phytoplankton community composition was dominated by diatoms across all depths, while cryptophytes were nearly absent (Fig. 6b). Four days later (16 January 2019), there was a clear increase in the concentration of chl-*a* (from ~5 to ~11.5 mg $m^{-3}$ at surface), primarily due to the biomass accumulation of diatoms associated with MLD of 26 m (Fig. 6a, b). However, on January 31, coinciding with enhanced stratification and shallower MLD (13 m), surface concentration of chl-*a* considerably decreased (< 2 mg $m^{-3}$ at surface) along with the diatom proportion, which was markedly replaced by cryptophytes (over 30%; Fig. 6b). At this station, there was a substantial decrease in both $\Delta p\mathrm{CO_2}$ (from –30 to –78 μatm) and $p\mathrm{CO_2}^{\mathrm{nonT}}$ (from ~375 to 323 μatm) from the first to the second sampling period (12 and 16 January, respectively), during which diatoms accounted for more than 97% of the total chl-*a* at both times. In contrast, during the third sampling period, substantially higher $\Delta p\mathrm{CO_2}$ (–12 μatm) was observed.

### 3.6.2. Gerlache Strait

A significant presence of cryptophytes was observed at St. G12 and St. G13 (Fig. 7). Across all sampling periods, cryptophytes consistently contributed over 70% in respect to the phytoplankton community composition at both stations (Fig. 7a). In the first sampling day (25 January 2019) at St. G12, the absolute contribution of cryptophytes on surface was approximately 3.1 mg $m^{-3}$, decreasing to 2.1 mg $m^{-3}$ by the time of the second sampling (30 January 2019) (Fig. 7a). Between the periods, $p\mathrm{CO_2}^{\mathrm{nonT}}$ and $\Delta p\mathrm{CO_2}$ decreased slightly, by 9 μatm and 8 μatm, respectively. At St. G13, cryptophytes had a biomass increase from 2.4 mg $m^{-3}$ (on 25 January 2019) to 3.3 mg $m^{-3}$ (on 30 January 2019; Fig. 7a). Correspondingly, $p\mathrm{CO_2}^{\mathrm{nonT}}$ and $\Delta p\mathrm{CO_2}$ decreased by 4 μatm and 10 μatm, respectively. At both stations, there were no significant changes in upper ocean stratification over the sampling period (Figs. 6b and 7b).

## 4. Discussion

### 4.1. Environmental factors, phytoplankton community, and $CO_2$ drawdown

This study revealed a well–defined gradient in surface environmental patterns along the NAP, reflecting distinct biogeochemical and oceanographic contrasts among the six subregions (Fig. 2b,c; Fig. 3). In spring and summer, environmental conditions are favourable for phytoplankton growth. As phytoplankton take up carbon during photosynthesis, higher chlorophyll-*a* concentrations are usually associated with lower $\Delta p\mathrm{CO_2}$ values (Kerr et al. 2018b, Brown et al. 2019, Costa et al. 2020). For example, exceptional low $\Delta p\mathrm{CO_2}$ values (up to –250 µatm) were recorded during an intense summer diatom bloom (> 45 mg $m^{-3}$ of chl-*a*) in the Gerlache Strait in February 2016 (Costa et al. 2020). Therefore, large phytoplankton blooms have critical role in driving the oceanic $CO_2$ sink via the biological carbon pump (Tréguer et al. 2018).

Diatoms are typically the primary drivers of significant $CO_2$ sequestration in Antarctic coastal waters (Brown et al. 2019, Costa et al. 2020, 2021). These organisms are the major contributor in the biological carbon pump and compound a fundamental group for the silica cycling (Tréguer et al. 2000). Nonetheless, several studies have reported an increasing prevalence of cryptophytes, which are overlapping diatoms in Antarctic Peninsula coastal waters, particularly in regions influenced by glacial melting (e.g., Moline et al. 2004, Mendes et al. 2013, 2018b, 2023). These studies have highlighted a clear competition or niche segregation between cryptophytes and diatoms, driven by physical and chemical properties of the water column, with cryptophytes being found more frequently in shallower and less saline waters (Mendes et al. 2023). We found similar results in this study, with cryptophytes accumulating biomass in the Gerlache Strait (Fig. 2d,e), where the highest meltwater percent was recorded in association with low salinity values and shallow mixing layers (Fig. 3). The Gerlache Strait and Continental Weddell subregions were observed as ocean $CO_2$ sink zones, although the phytoplankton community composition was different between both subregions (Fig. 2d,e). Diatoms were predominant in the Continental Weddell, while cryptophytes dominated in the Gerlache Strait. Thus, the lower $\Delta p\mathrm{CO_2}$ and higher $CO_2$ uptake over the Continental Weddell are consistent with the hypothesis that diatoms are more efficient than cryptophytes for oceanic $CO_2$ uptake (e.g., Brown et al. 2019).

The Bransfield Strait subregion acted as a net $CO_2$ source to the atmosphere, showing greater variability in $\Delta p\mathrm{CO_2}$ ($7 \pm 31$ µatm) and a higher $\mathrm{FCO_2}$ ($1.16 \pm 2.65$ mmol $m^{-2}$ $day^{-1}$) compared to the Drake Passage and Bellingshausen Sea subregions. Such variability in $\Delta p\mathrm{CO_2}$ was explained by processes other than temperature changes, as there was no difference between $p\mathrm{CO_2}^{\mathrm{nonT}}$ and $p\mathrm{CO_2}^{\mathrm{sw}}$ (Fig. 4). The significantly negative correlation ($r^2 = 0.5$ and $p < 0.001$) between chl-*a* and $\Delta p\mathrm{CO_2}$ (Supplementary Material Table S3) suggested that phytoplankton biomass is an important driver modulating sea–air $CO_2$ exchanges in the Bransfield Strait subregion. The highest chl-*a* value was registered in the Bransfield Strait (11.26 mg $m^{-3}$), however, it was observed in an isolated station, concurrent with a strong $CO_2$ uptake ($\Delta p\mathrm{CO_2} = -78$ µatm). In contrast, the other stations in the Bransfield Strait showed surface chl-*a* values around 2 mg $m^{-3}$. The large spatial dimension and the high variability of surface chl-*a* (from 0.35 to 11.26 mg $m^{-3}$) along Bransfield Strait, hence, may be associated with the net $CO_2$ release to the atmosphere found in January 2019. Indeed, Kerr et al. (2025) showed that, in the Bransfield Strait during summer 2019, although photosynthesis drove $CO_2$ variability throughout the region, dominant net respiration led the area to act as a net $CO_2$ source.

Over a short time scale (i.e., one week), a shift from diatoms to cryptophytes was observed in the Bransfield Strait, coinciding with a shallowing MLD (from 24 m to 13 m) and increased meltwater input (from ~ 0.23% to ~ 1%). This shift in phytoplankton community composition was reflected in a noticeable decrease in $\Delta p\mathrm{CO_2}$ values (Fig. 6). On the other hand, under persistent water column stratification over a course of one week, there was no clear change in phytoplankton community composition and $\Delta p\mathrm{CO_2}$ in the Gerlache Strait subregion, where cryptophytes were dominating (Fig. 7). These results suggest that the water column structure in Gerlache Strait was more stable in a scale of week than that observed in Bransfield Strait. Changes in water column structure clearly favoured shifts in phytoplankton community composition and thus differences in oceanic $CO_2$ uptake. These findings also underscore that the temporal scale of biogeochemical processes can play a fundamental role in characterising regions as variable as the NAP. Exploring this temporal variability in future studies will be essential for a more accurate and comprehensive biogeochemical assessment of the region.

With the lowest temperature and the highest proportion of diatoms, the Continental Weddell subregion exhibited the strongest $CO_2$ undersaturation in January 2019. The relationship between $CO_2$ uptake and chl-*a* ($\Delta p\mathrm{CO_2}$ to chl-*a*) in the Continental Weddell was six– and four–fold higher than the relationships recorded in the Bransfield and Gerlache Straits, respectively (Supplementary Material Table S3). Although phytoplankton biomass in the Continental Weddell (maximum chl-*a* of 2.35 mg $m^{-3}$) did not reach bloom levels as observed in the Bransfield Strait, the region acted, on average, as a strong $CO_2$ sink, while the Bransfield Strait acted as a $CO_2$ source to the atmosphere. This intense $CO_2$ uptake may provide further evidence that diatom dominance plays a key role in carbon dynamics. For instance, photosynthesis was identified as the main driver of DIC changes in the Antarctic Sound during summer 2019, when the highest surface oxygen supersaturation across the NAP was also recorded (Kerr et al. 2025, Monteiro et al. 2025). In addition, this region showed elevated carbonate ion concentrations and high pH (Monteiro et al. 2025), both typical features of phytoplankton growth in polar waters (Fransson et al. 2013, Monteiro et al. 2025). The strong $CO_2$ uptake was further enhanced by increased solubility in the colder waters of the area (Monteiro et al. 2025). Moreover, the Continental Weddell was the subregion that had the highest grazing index (reaching 23%), indicating that intense zooplankton grazing pressure occurred (based on a reference value of 10%; Mendes et al. 2012). The zooplankton faecal pellets derived from intense feeding activity may further contribute for the local biological carbon pump, as the heavy faecal pellets concentrate phytoplankton cells increasing the organic matter sinking process out of the upper layers (Henley et al. 2020).

In contrast, the Oceanic Weddell presented higher values of senescence index (up to 10%), indicating that the local phytoplankton community could be under unfavourable conditions (Costa et al. 2021), likely associated with micronutrient limiting concentrations (Mendes et al. 2012). In the Oceanic Weddell, where phytoplankton biomass accumulation was low, the observed sea–air $CO_2$ exchanges appeared to be primarily driven by the seasonal dynamics of sea ice – particularly its melting and formation – underscoring the role of physical processes in modulating carbonate system variability in this region (Fig. 5), likely due to increased $CO_2$ solubility in colder, less saline waters (Fig. 2c). Indeed, the Oceanic Weddell was the only subregion where the $\Delta$Alk:$\Delta$DIC ratio clearly reflected a strong influence of non-biological processes (i.e., other than photosynthesis/respiration) affecting both Alk and DIC (Fig. 5). This area also showed the highest T:nonT ratio (Fig. 4), suggesting a greater relative influence of thermal processes on $pCO_2^{sw}$ change compared to the other NAP subregions. Nevertheless, $\Delta$Alk:$\Delta$DIC ratios, which differ from the theoretical values expected for each process, suggest that multiple processes act simultaneously to influence changes in the marine carbonate system along the northern Antarctic Peninsula (e.g., Monteiro et al. 2020b). Even in regions with a strong correlation between chl-*a* and $\Delta pCO_2$, the observed slope of the nitrate–DIC relationship was 0.06 (Fig. S1 in the Supplementary Material), rather than the expected 0.14 for nitrate uptake or release relative to DIC during photosynthesis or respiration (Yin et al. 2024). This suggests that multiple processes are acting simultaneously.

The Drake Passage is a transition zone, characterised by deep water currents and intense geomorphological processes (Bohoyo et al. 2018). From 2003 to 2015, Munro et al. (2015)

observed an increase of –0.37 ± 0.16 μatm $yr^{-1}$ in the magnitude of $\Delta p\text{CO}_2$ in the Drake Passage, indicating a strengthening in the ocean $CO_2$ sink. Nonetheless, large spatial and interannual variability in the magnitude of sea–air $CO_2$ exchange has been found in the Drake Passage (Ito et al. 2018, Arbilla et al. 2024). Here, $\Delta p\text{CO}_2$ was positive in the Drake Passage, likely indicating a source of $CO_2$ towards the atmosphere in January 2019, despite diatom proportion being > 50% and chl-*a* reaching 2 mg $m^{-3}$ (Fig. 2e and Supplementary Material Table S3). This was similarly observed in the Bellingshausen Sea subregion, where there was a relative release of $CO_2$ associated with high proportion of diatoms (> 50%; Fig. 2e) and chl-*a* of up to 2.2 mg $m^{-3}$. Such result is intriguing as diatoms are known to uptake $CO_2$ more efficiently than the other phytoplankton groups (Brown et al. 2019). Probably, the local upwelling of CDW-derived rich $CO_2$ waters along the Drake Passage and Bellingshausen Sea may be influencing $p\text{CO}_2^{sw}$ dynamics (Kerr et al. 2025), counteracting the effect of photosynthesis on reducing $\Delta p\text{CO}_2$. It is worth noting that the region of the Drake Passage addressed in the present study encompasses only a limited set of stations located on the continental shelf surrounding the northeastern part of Elephant Island – in the southernmost sector of the Drake Passage.

### 4.2. Diatom taxa modulating sea–air $CO_2$ exchanges

Diatoms form the foundation of the Antarctic trophic web and play a critical role in the biological carbon pump (Tréguer et al. 2018, Brown et al. 2019, Costa et al. 2020, 2021). Over evolutionary time, a distinction has arisen between centric and pennate diatoms, with pennate diatoms generally exhibiting greater diversification than centric ones (Finkel et al. 2005). Pennate diatoms are also characterised by a further reduction in frustule size and dimensions compared to centric diatoms (Finkel et al. 2005). Cell size is recognised as an important factor for processes such as atmospheric carbon sequestration (Laws 2000; Finkel et al. 2010).

Phytoplankton communities dominated by larger cells tend to support more efficient energy transfer throughout the food web and enhance the export of fixed carbon (Mouw et al. 2016, Serra-Pompei et al. 2022).

Diatom taxa were different over the subregions in January 2019 (Table S2 in the Supplementary Material). Although diatoms showed predominantly high proportions (> 50%) in the Continental Weddell and Bransfield Strait subregions, the diatom species was different between both subregions. While in the Bransfield Strait there was a substantial contribution of pennate diatoms (e.g., *Fragilariopsis* spp. and *Pseudo–nitzschia* sp.), a greater contribution of centric ones (e.g., *Chaetoceros* sp. and *Thalassiosira* spp.) was observed in the Continental Weddell. Although centric diatoms had high density in the Bransfield Strait, their contribution was much higher in the Continental Weddell subregion, where pennate diatoms were nearly absent (Supplementary Material Table S2). Thus, although further studies are still needed, it is plausible to hypothesise that the observed $\Delta p\mathrm{CO_2}$ differences between the Bransfield Strait and the Continental Weddell subregions may be linked to variations in the dominant diatom species. Similarly, while the presence of high densities of *Pseudo-nitzschia* sp. in the Drake Passage and Bellingshausen Sea (see Table S2 in the Supplementary Material) coincides with areas of net $CO_2$ outgassing, additional data are required to determine whether the dominance of this diatom directly influences carbon fluxes. At this stage, such a link remains hypothetical. Overall, the remarkable diversity of diatoms observed along the northern Antarctic Peninsula (Costa et al. 2022) may contribute to the spatial variability of regional biogeochemical processes. Such diversity, reflected in the distinct composition and dominance patterns between subregions, could influence primary production dynamics and carbon fluxes.

Despite having the highest average chl-*a* concentration among the NAP subregions, the Gerlache Strait subregion did not correspondingly exhibit the largest $CO_2$ uptake. The average chl-*a* concentration in the Gerlache Strait was more than the double of that recorded in the

Continental Weddell, where the highest $CO_2$ uptake was observed. Unlike the Continental Weddell subregion, cryptophytes were the dominant phytoplankton group in the Gerlache Strait. The $CO_2$ uptake efficiency found in the Gerlache Strait under a predominant contribution of cryptophytes was much lower than that found in the Continental Weddell, associated with high contribution of centric diatoms. These observations reinforced previous localised studies conducted along the western Antarctic Peninsula that have found a lower efficiency in oceanic $CO_2$ uptake of cryptophytes compared with the diatoms (Kerr et al. 2018b, Brown et al. 2019).

Overall, we provide multiple field-based lines of evidence supporting the hypothesis that dominant phytoplankton groups, even at the species level, play distinct roles in oceanic $CO_2$ dynamics. For instance, we observed marked variability in salinity-normalised DIC across sampling times in the Bransfield Strait. When diatoms accounted for 97–98% of the phytoplankton community, normalised DIC decreased from 2175 $\mu$mol kg$^{-1}$ at chl-*a* levels of 5 mg m$^{-3}$ to 2155 $\mu$mol kg$^{-1}$ when chl-*a* increased substantially to 11.5 mg m$^{-3}$. DIC rose to 2181 $\mu$mol kg$^{-1}$ as chl-*a* dropped sharply to 2 mg m$^{-3}$, coinciding with a more diverse community composed of 44% diatoms, 28% cryptophytes, 14% *Phaeocystis antarctica* and 12% dinoflagellates. Conversely, salinity-normalised Alk remained stable at around 2304 $\mu$mol kg$^{-1}$ across all three sampling periods. These results strengthen the conclusion that the observed DIC and $pCO_2$ drawdown were indeed driven by phytoplankton growth, particularly diatoms, as physical processes would have also altered Alk. Furthermore, since laboratory experiments on this topic are complex and difficult to obtain, the comparison between stations dominated by centric diatoms with those dominated by pennate diatoms can provide a unique opportunity to better understand differences in their roles in $CO_2$ uptake. Long-term studies with extensive time series will be essential to evaluate the relative effectiveness of centric and pennate diatoms in driving oceanic $CO_2$ uptake. Despite the complexity of the topic at hand, our results suggest that, in addition to biomass accumulation, species composition could be a key factor influencing $CO_2$ uptake.

## 5. Concluding remarks

In this study, we have subdivided the NAP into six biogeochemically distinct subregions using an extensive dataset collected in January 2019. Our findings suggested non–thermal processes, such as phytoplankton growth and ocean dynamics, were the primary drivers of sea–air $CO_2$ differences in all subregions. Furthermore, we observed that phytoplankton community composition plays a crucial role on the magnitudes of sea–air $CO_2$ differences. In particular, $CO_2$ uptake was strongest under diatom dominance, while regions dominated by cryptophytes showed a reduced ocean-atmosphere $CO_2$ flux into the ocean. Future studies should therefore focus on the specific effects of phytoplankton species on oceanic $CO_2$ uptake. Understanding sea–air $CO_2$ exchanges in species resolution will be crucial for better predicting biogeochemical processes in models of Antarctic coastal regions, especially in rapidly warming areas such as the NAP.

## Declaration of competing interest

The authors declare that they have no known competing financial interests or personal relationships that could have appeared to influence the work reported in this paper.

## Data availability

Data will be made available on request.

## Acknowledgments

This is a multidisciplinary study as part of the Brazilian High Latitude Oceanography Group (GOAL) activities in the Brazilian Antarctic Program (PROANTAR). Financial support was provided by National Council for Research and Development (CNPq) and Coordination for the Improvement of Higher Education Personnel (CAPES). This study was conducted within the activities of the PROVOCCAR, ECOPELAGOS, PRO–SAMBA and IMPACTANT (CNPq grant numbers 442628/2018–8, 442637/2018–7, 440859/2023–9, 440865/2023–9, respectively) projects. The authors thank the crew of the RV Almirante Maximiano of the Brazilian Navy and several scientists and technicians participating in the cruise for their valuable help during sampling. We are grateful to Simon Wright, from the Australian Antarctic Division, for providing the CHEMTAX v.1.95 software; and to Chariane Werlang and Ana Paula Costa, from Federal University of Rio Grande, for their help with the microscopic analyses. A MSc fellowship from CAPES was granted to R.R. Costa. A. Ferreira received a PhD grant (SFRH/BD/144586/2019) and a contract from the Scientific Employment Stimulus Programme (2024.10305.CEECIND) from Fundação para a Ciência e a Tecnologia (FCT). C.R.B. Mendes, R. Kerr, E.R. Secchi and T. Monteiro (PDJ grant No. 171829/2023-9) are granted research fellowships from CNPq. CAPES also provided free access to many relevant journals through the portal "Periódicos CAPES". This study also received additional from the FCT through the strategic project UIDB/04292/2020 (doi: 10.54499/UIDB/04292/2020) and UIDP/04292/2020 (doi: 10.54499/UIDP/04292/2020) awarded to MARE and through project LA/P/0069/2020 (doi: 10.54499/LA/P/0069/2020) granted to the Associate Laboratory ARNET, as well as through the Portuguese Polar Program (PROPOLAR). This study is within the scope of two Projects of the Institutional Internationalization Program (Capes PrInt–FURG –Edital 41/2017). This research is also framed within the College on Polar and Extreme Environments (Polar2E) of the University of Lisbon. For the purpose of open access, the

author(s) has applied a Creative Commons attribution (CC BY) licence to any Author Accepted Manuscript version arising.

## References

Ackley SF, Buck KR, Taguchi S (1979) Standing crop of algae in the sea ice of Weddell Sea region. Deep-Sea Research Part I 26: 269–281. https://doi.org/10.1016/0198-0149(79)90024-4

Aminot A, Chaussepied M (1983) Manuel des analyses chimiques em Milieu Marin. CNEXO, Brest.

Arbilla LA, Ruiz-Etcheverry LA, López-Abbate C, Kahl LC (2024) $CO_2$ sink and source zones delimited by marine fronts in the Drake Passage. Progress in Oceanography 223: 103246. https://doi.org/10.1016/j.pocean.2024.103246

Barlett EMR, Tosonotto GV, Piola AR, Sierra ME, Mata MM (2018) On the temporal variability of intermediate and deep waters in the Western Basin of the Bransfield Strait. Deep-Sea Research Part II: Tropical Studies in Oceanography 149: 31–46. https://doi.org/10.1016/j.dsr2.2017.12.010

Bittig HC, Steinhoff T, Claustre H, Fiedler B, Williams NL, Sauzède R, Körtzngер A, Gattuso JP (2018) An Alternative to Static Climatologies: Robust Estimation of Open Ocean $CO_2$ Variables and Nutrient Concentrations From T, S, and $O_2$ Data Using Bayesian Neural Networks. Frontiers Marine Science 5: 328. https://doi.org/10.3389/fmars.2018.00328

Bohoyo F, Larter RD, Galindo-Zaldívar J, Leat PT, Maldonado A, Tate AJ, Flexas MM Gowland EJM, Arndt JE, Dorschel B, Kim YD, Hong JK, Martínez-López J, Maestro, Bermúdez O, Nitsche FO, Livermore RA, Riley TR (2018) Morphological and geological features of Drake Passage, Antarctica, from a new digital bathymetric model. Journal of Maps 15: 49–59. https://doi.org/10.1080/17445647.2018.1543618

Brown MS, Munro DR, Feehan CJ, Sweeney C, Ducklow HW, Schofield OM, (2019) Enhanced oceanic $CO_2$ uptake along the rapidly changing West Antarctic Peninsula. Nature Climate Change 9: 678–683. https://doi.org/10.1038/s41558-019-0552-3

Canuti E, Artuso F, Bracher A, Brotas V, Devred E, Dimier C, Giardina I, Mendes CRB, Murawski S, Peeken I, Tracana A, Ras J, Wiegmann S (2022) The Fifth HPLC Intercomparison on Phytoplankton Pigments (HIP-5). Publications Office of the European Union, Luxembourg.

Cao Z, Yang W, Zhoa Y, Guo X, Yin Z, Du C, Zhoa H, Dai M (2020) Diagnosis of $CO_2$ dynamics and fluxes in global coastal oceans. National Science Review 7: 786–797. https://doi.org/10.1093/nsr/nwz105

Carvalho ACO, Kerr R, Tavano VM, Mendes CRB (2022) The southwestern South Atlantic continental shelf biogeochemical divide. Biogeochemistry 159: 139–158. https://doi.org/10.1007/s10533-022-00918-8

Collares LL, Mata MM, Kerr R, Arigony-Neto J (2018) Iceberg drift and ocean circulation in the northwestern Weddell Sea, Antarctica. Deep-Sea Research Part II 149: 10–24. https://doi.org/10.1016/j.dsr2.2018.02.014

Cook AJ, Holland PR, Meredith MP, Murray T, Luckman A, Vaughan DG (2016) Ocean forcing of glacier retreat in the western Antarctic Peninsula. Science 353: 283–286. https://www.science.org/doi/10.1126/science.aae0017

Costa RR, Mendes CRB, Tavano VM, Dotto TS, Kerr R, Monteiro T, Odebrecht C, Secchi ER, (2020) Dynamics of an intense diatom bloom in the Northern Antarctic Peninsula, February 2016. Limnology and Oceanography 65: 2056–2075. https://doi.org/10.1002/lno.11437

Costa RR, Mendes CRB, Ferreira A, Tavano VM, Dotto TS, Secchi ER (2021) Large diatom bloom off the Antarctic Peninsula during cool conditions associated with the 2015/2016 El Niño. Communications Earth & Environment 2: 1–11. https://doi.org/10.1038/s43247-021-00322-4

Costa RR, Mendes CRB, Souza MS, Tavano VM, Secchi ER (2022) Chemotaxonomic characterization of the key genera of diatoms in the Northern Antarctic Peninsula. Annals of the Brazilian Academy of Sciences 94: e20210584. https://doi.org/10.1590/0001-3765202220210584

Costa RR, Ferreira A, Souza MS, Tavano VM, Kerr R, Secchi ER, Brotas V, Dotto TS, Brito AC, Mendes CRB (2023) Physical-biological drivers modulating phytoplankton seasonal succession along the Northern Antarctic Peninsula. Environmental Research 231: 116273. https://doi.org/10.1038/s43247-021-00322-4

Damini BY, Costa RR, Dotto TS, Mendes CRB, Torres-Lasso JC, Azaneu MVC, Mata MM, Kerr R (2023) Antarctica Slope Front bifurcation eddy: A stationary feature influencing $CO_2$ dynamics in the northern Antarctic Peninsula. Progress in Oceanography 212: 102985. https://doi.org/10.1016/j.pocean.2023.102985

Damini BY, Brum AL, Hall RA, Dotto TS, Azevedo JLL, Heywood KJ, Mata MM, Garcia CAE, Kerr R (2025) Summer circulation and water masses transport in Bransfield Strait, Antarctica: An evaluation of their response to combined effects of Southern Annular Mode and

El Niño–Southern Oscillation. Deep-Sea Research Part I: Oceanographic Research Papers 222: 104516. https://doi.org/10.1016/j.dsr.2025.104516

de Boyer Montégut C, Madec G, Fischer AS, Lazar A, Iudicone D (2004) Mixed layer depth over the global ocean: An examination of profile data and a profile-based climatology. Journal of Geophysical Research: Oceans 109: 1–20. https://doi.org/10.1029/2004JC002378

Dotto TS, Kerr R, Mata MM, Garcia CAE (2016) Multidecadal freshening and lightening in the deep waters of the Bransfield Strait, Antarctica. Journal of Geophysical Research: Oceans 121: 3741–3756. https://doi.org/10.1002/2015JC011228

Ferreira A, Costa RR, Dotto TS, Kerr R, Tavano VM, Brito AC, Brotas V, Secchi ER, Mendes CRB (2020) Changes in phytoplankton communities along the Northern Antarctic Peninsula: causes, impacts and research priorities. Frontiers in Marine Science 7: 576254. https://doi.org/10.3389/fmars.2020.576254

Finkel ZV, Katz ME, Wright JD, Schofield OME, Falkowski PG (2005) Climatically driven macroevolutionary patterns in the size of marine diatoms over the Cenozoic. Proceedings of the National Academy of Sciences 102: 8927–8932. https://doi.org/10.1073/pnas.0409907102

Finkel ZV, Kotrc B (2010) Silica Use Through Time: Macroevolutionary Change in the Morphology of the Diatom Frustule. Geomicrobiology Journal 27: 596–608. https://doi.org/10.1080/01490451003702941

Fransson A, Chierici M, Miller LA, Carnat G, Shadwick E, Thomas H, Papakyriakou TN (2013) Impact of sea-ice processes on the carbonate system and ocean acidification at the ice-water interface of the Amundsen gulf, Arctic Ocean. Journal of Geophysical Research: Oceans 118: 7001–7023. https://doi.org/10.1002/2013JC009164

Friis K, Körtzinger A, Wallace DW (2003) The salinity normalization of marine inorganic carbon chemistry data. Geophysical Research Letters, 30: 1085. https://doi.org/10.1029/2002GL015898

Grasshoff K, Kremling K, Ehrhardt M (2009) Methods of Seawater Analysis, third ed. WILEY-VCH, Weinheim.

Hauri C, Doney SC, Takahashi T, Erickson M, Jiang G, Ducklow HW (2015) Two decades of inorganic carbon dynamics along the West Antarctic Peninsula. Biogeosciences 12: 6761–6779. https://doi.org/10.5194/bg-12-6761-2015

Henley SF, Cavan EL, Fawcett SE, Kerr R, Monteiro T, Sherrell RM, Bowie AR, Boyd PW, Barnes DKA, Schloss IR, Marshall T, Flynn R, Smith S (2020) Changing biogeochemistry of the Southern Ocean and its ecosystem implications. Frontiers in Marine Science 7: 581. https://doi.org/10.3389/fmars.2020.00581

Hersbach H, Bell B, Berrisford P, Hirahara S, Horányi A, Muñoz-Sabater J, Nicolas J, Peubey C, Radu R, Schepers D, Simmons A, Soci C, Abdalla S, Abellan X, Balsamo G, Bechtold P, Biavati G, Bidlot J, Bonavita M, De Chiara G, Dahlgren P, Dee D, Diamantakis M, Dragani R, Flemming J, Forbes R, Fuentes M, Geer A, Haimberger L, Healy S, Hogan RJ, Hólm E, Janisková M, Keeley S, Laloyaux P, Lopez P, Lupu C, Radnoti G, de Rosnay P, Rozum I, Vamborg F, Villaume S, Thépaut JN (2020) The ERA5 global reanalysis. Quarterly Journal of the Royal Meteorological Society 146: 1999–2049. https://doi.org/10.1002/QJ.3803

Huot Y, Babin M, Bruyant F, Grob C, Twardowski MS, Claustre H (2007) Relationship between photosynthetic parameters and different proxies of phytoplankton biomass in the subtropical ocean. Biogeosciences 4: 853–868. https://doi.org/10.5194/bg-4-853-2007

Ito RG, Tavano VM, Mendes CRB, Garcia CAE (2018) Sea-air $CO_2$ fluxes and $pCO_2$ variability in the Northern Antarctic Peninsula during three summer periods (2008-2010). Deep-Sea Research Part II 149: 84–98. https://doi.org/10.1016/j.dsr2.2017.09.004

Jeffrey SW (1974) Profiles of photosynthetic pigments in the ocean using thin-layer chromatography. Marine Biology 26: 101–1110. https://doi.org/10.1007/BF00388879

Kerr R, Mata MM, Mendes CRB, Secchi ER (2018a) Northern Antarctic Peninsula: a marine climate hotspot of rapid changes on ecosystems and ocean dynamics. Deep-Sea Research Part II 149: 4–9. https://doi.org/10.1016/j.dsr2.2018.05.006

Kerr R, Dotto TS, Mata MM, Hellmer HH (2018b). Three decades of deep-water mass investigation in the Weddell Sea (1984-2014): Temporal variability and changes. Deep-Sea Research Part II 149: 70–83. https://doi.org/10.1016/j.dsr2.2017.12.002

Kerr R, Monteiro T, Orselli IBM, Tavano VM, Mendes CRB (2024) Sea-air $CO_2$ exchanges, $pCO_2$ drivers and phytoplankton communities in the southwestern South Atlantic Ocean during spring. Marine Chemistry 267: 104472. https://doi.org/10.1016/j.marchem.2024.104472

Kerr R, Monteiro R, Batista M, Damini B (2025) Physical-biological processes regulating summer sea-air $CO_2$ exchanges along the Drake Passage and northern Antarctic Peninsula. Marine Chemistry 269: 104497. https://doi.org/10.1016/j.marchem.2025.104497

Lapierre JF, Guillemette F, Berggren M, del Giorgio PA (2017) Inland waters as drivers of carbon transport and processing in the biosphere. Nature Geoscience 10: 861–865.

Laws EA, Falkovski PG, Smith WO, Ducklow H, McCarthy J (2000) Temperature effects on export production in the open ocean. Global Biogeochemical Cycles 14: 1231–1246. https://doi.org/10.1029/1999GB001229

Mackey MD, Mackey DJ, Higgins HW, Wright SW (1996) CHEMTAX—a Program for Estimating Class Abundances from Chemical Markers: application to HPLC Measurements of Phytoplankton. Marine Ecology Progress 144: 265–283. https://doi.org/10.3354/meps144265

Mata MM, Tavano VM, Garcia CAE (2018) 15 years sailing with the Brazilian High Latitude Oceanography Group (GOAL). Deep-Sea Research Part II: Tropical Studies in Oceanography 149: 1–3. https://doi.org/10.1016/j.dsr2.2018.05.007

Mendes CRB, Cartaxana P, Brotas V (2007) HPLC determination of phytoplankton and microphytobenthos pigments: Comparing resolution and sensitivity of a C18 and a C8 method. Limnology and Oceanograph: Methods 5: 363–370. https://doi.org/10.4319/lom.2007.5.363

Mendes CRB, de Souza MS, Garcia VMT, Leal MC, Brotas V, Garcia CAE (2012) Dynamics of phytoplankton communities during late summer around the tip of the Antarctic Peninsula. Deep-Sea Research Part I 65: 1–14. https://doi.org/10.1016/j.dsr.2012.03.002

Mendes CRB, Tavano VM, Leal MC, de Souza MS, Brotas V, Garcia CAE (2013) Shifts in the dominance between diatoms and cryptophytes during three late summers in the Bransfield Strait (Antarctic Peninsula). Polar Biology 36: 537–547. https://doi.org/10.1007/s00300-012-1282-4

Mendes CRB, Tavano VM, Dotto TS, Kerr R, de Souza MS, Garcia CAE, Secchi ER (2018a). New insights on the dominance of cryptophytes in Antarctic coastal waters: a case study in Gerlache Strait. Deep-Sea Research Part II 149: 161–170. https://doi.org/10.1016/j.dsr2.2017.02.010

Mendes CRB, Tavano VM, Kerr R, Dotto TS, Maximiano T, Secchi ER (2018b) Impact of sea ice on the structure of phytoplankton communities in the northern Antarctic Peninsula. Deep-Sea Research Part II: Topical Studies in Oceanography 149: 111–123. https://doi.org/10.1016/j.dsr2.2017.12.003

Mendes CRB, Costa RR, Ferreira A, Jesus B, Tavano VM, Dotto TS, Leal MC, Kerr R, Islabão CA, Franco AOR, Mata MM, Garcia CAE, Secchi ER (2023) Cryptophytes: An emerging group in the rapidly changing Antarctic Peninsula marine environments. Global Change Biology 29: 1791–1808. https://doi.org/10.1111/gcb.16602

Moline MA, Claustre H, Frazer TK, Schofield O, Vernet M (2004) Alteration of the food web along the Antarctic Peninsula in response to a regional warming trend. Global Change Biology 10: 1973–1980. https://doi.org/10.1111/j.1365-2486.2004.00825.x

Monteiro T, Kerr R, Machado C (2020a) Seasonal variability of net sea air – $CO_2$ fluxes in a coastal region of the northern Antarctic Peninsula. Science Reports 10: 14875. https://www.nature.com/articles/s41598-020-71814-0

Monteiro T, Kerr R, Orselli IBM, Lencina-Avila JM (2020b) Towards an intensified summer $CO_2$ sink behaviour in the Southern Ocean coastal regions. Progress in Oceanography 183: 102267. https://doi.org/10.1016/j.pocean.2020.102267

Monteiro T, Henley SF, Pollery RCG, Mendes CRB, Mata MM, Tavano VM, Garcia CAE, Kerr R (2023) Spatiotemporal variability of dissolved inorganic macronutrients along the northern Antarctic Peninsula (1996-2019). Limnology and Oceanography 68: 2305–2326. https://doi.org/10.1002/lno.12424

Monteiro T, Batista MS, Kerr R (2025) Spatial variability of marine carbonate system along the Drake Passage and northern Antarctic Peninsula during the austral summer. Marine Chemistry 271: 104529. https://doi.org/10.1016/j.marchem.2025.104529

Moreth CM, Yentsch CS (1970) The role of chlorophyllase and light in the decomposition of chlorophyll from marine phytoplankton. Journal of Experimental Marine Biology Ecology 4: 238–249. https://doi.org/10.1016/0022-0981(70)90037-7

Mouw CB, Barnett A, McKinley GA, Gloege L, Pilcher D (2016) Phytoplankton size impact on export flux in the global ocean. Global Biogeochemical Cycles 30: 1542–1562. https://doi.org/10.1002/2015GB005355

Munro DR, Lovenduski NS, Takahashi T, Stephens BB, Newberger T, Sweeney C (2015) Recent evidence for a strengthening $CO_2$ sink in the Southern Ocean from carbonate system measurements in the Drake Passage (2002-2015). Geophysical Research Letters 42: 7623–7630. https://doi.org/10.1002/2015GL065194

Orr JC, Epitalon JM, Dickson AG, Gattuso JP (2018) Routine uncertainty propagation for the marine carbon dioxide system. Marine Chemistry 207: 84–107. https://doi.org/10.1016/j.marchem.2018.10.006

Orselli IBM, Carvalho ACO, Monteiro T, Damini BY, De Carvalho MB, Albuquerque C, Kerr R (2022) The marine carbonate system along the northern Antarctic Peninsula: current knowledge and future perspectives. Anais da Academia Brasileira de Ciências 94: 20210825. https://doi.org/10.1590/0001-3765202220210825

Pierrot D, Lewis E, Wallace DWR (2006) MS Excel Program Developed for $CO_2$ System Calculations, ORNL/CDIAC-105a. Oak Ridge National Laboratory, Oak Ridge.

Rivaro P, Messa R, Ianni C, Magi E, Budillon G (2014) Distribution of total alkalinity and pH in the Ross Sea (Antarctica) waters during austral summer 2008. Polar Research 33: 1–45. https://doi.org/10.3402/polar.v33.20403

Rost B, Riebesell U, Burkhardt S, Sültemeyer D (2003) Carbon acquisition of bloom-forming marine phytoplankton. Limnology and Oceanography, 48: 55–67. https://doi.org/10.4319/lo.2003.48.1.0055

Rysgaard S, Bendtsen J, Dilille B, Dieckmann GS, Glud RN, Kennedy H, Mortensen J, Papadimitriou S, Thomas DN, Tison J-L (2001) Sea ice contribution to the air-sea $CO_2$ exchange in the Arctic and Southern Oceans. Tellus B: Chemical and Physical Meteorology 63: 823–830. https://b.tellusjournals.se/articles/10.1111/j.1600-0889.2011.00571.x

Santos-Andrade M, Kerr R, Orselli IB, Monteiro T, Mata MM, Goyet C (2023) Drivers of Marine $CO_2$-Carbonate Chemistry in the Northern Antarctic Peninsula. Global Biogeochemical Cycles 37: e2022GB007518. https://doi.org/10.1029/2022GB007518

Sarma VVSS, Prasad MHK, Dalabehera HB (2021) Influence of phytoplankton pigment composition and primary production on $pCO_2$ levels in the Indian Ocean. Journal of Earth System Science 130: 85. https://doi.org/10.1007/s12040-021-01598-y

Scott FJ, Marchant HJ (2005) Antarctic Marine Protists. Australian Biological Resources Study, Camberra.

Serra-Pompei C, Ward BA, Pinti J, Visser AW, Kiørboe T, Andersen KH (2022) Linking Plankton Size Spectra and Community Composition to Carbon Export and Its Efficiency. Global Biogeochemical Cycles 36: e2021GB007275. https://doi.org/10.1029/2021GB007275

Shaman FR, Lorenzen CJ (1975) Quantitative degradation of chlorophyll by a marine herbivore. Limnology and Oceanography 20: 580–586. https://doi.org/10.4319/lo.1975.20.4.0580

Signorini SR, McClain CR, Christian JR, Wong CS (2001) Seasonal and interannual variability of phytoplankton, nutrients, $TCO_2$, $pCO_2$, and $O_2$ in the eastern subarctic Pacific (ocean weather station Papa). Journal of Geophysical Research 106: 31197–31216. https://doi.org/10.1029/2000JC000343

Sournia A (1978) Phytoplankton manual. UNESCO, Paris.

Takahashi T, Sutherland SC, Sweeney C, Poisson A, Metzl N, Tilbrook B, Bates NR, Wanninkhof R, Feely RA, Sabine CL, Olafsson J, Nojiri Y (2002) Global sea–air $CO_2$ flux based on climatological surface ocean $pCO_2$, and seasonal biological and temperature effects. Deep-Sea Research Part II 49: 1601–1622. https://doi.org/10.1016/S0967-0645(02)00003-6

Takahashi T, Sutherland SC, Wanninkhof R, Sweeney C, Feely RA, Chipman DW, Hales B, Friederich G, Chavez FP, Sabine CL, Watson AJ, Bakker DCE, Schuster U, Metzl N, Yoshikawa-Inoue H, Ishii M, Midorikawa T, Nojiri Y, Körtzinger A, Steinhoff T, Hoppema M, Olafsson J, Arnarson TS, Tilbrook B, Johannessen T, Olsen A, Bellerby RGJ, Wong CS, Delille B, Bates NR, de Baar HJW (2009) Climatological mean and decadal change in surface ocean $pCO_2$, and net sea–air $CO_2$ flux over the global oceans. Deep-Sea Research Part II 56: 554–577. https://doi.org/10.1016/j.dsr2.2008.12.009

Ter Braak CJF, Prentice IC (1988) A Theory of Gradient Analysis. Advances in Ecological Research 181: 271–317. https://doi.org/10.1016/S0065-2504(08)60183-X

Testa G, Piñones A, Castro LR (2021) Physical and Biogeochemical Regionalization of the Southern Ocean and the CCAMLR Zone 48.1. Frontiers in Marine Science 8: 592378. https://doi.org/10.3389/fmars.2021.592378

Tréguer P, Pondaven P (2000) Silica control of carbon dioxide. Nature 406: 358–359. https://doi.org/10.1038/35019236

Tréguer P, Bowler C, Moriceau B, Dutkiewicz S, Gehlen M, Aumont O, Bittner L, Dugdale R, Finkel Z, Iudicone D, Jahn O, Guidi L, Lasbleiz M, Leblanc K, Levy M, Pondaven P (2018) Influence of diatom diversity on the ocean biological carbon pump. Nature Geoscience 11: 27–37. http://doi.org/10.1038/s41561-017-0028-x

Turner JS, Munro DR, Fay A, Stammerjohn S, Kim H, Schofield O, Dierssen H (2025) Seasonal variability of surface ocean carbon uptake and chlorophyll-a concentration in the West Antarctic Peninsula over two decades. Geophysical Research Letters 52: e2024GL112446. https://doi.org/10.1029/2024GL112446

Utermöhl H (1958). Zur vervollkommnung der quantitativen phytoplankton-methodik: Mit 1 Tabelle und 15 abbildungen im Text und auf 1 Tafel. Internationale Vereinigung für theoretische und angewandte Limnologie: Mitteilungen 9: 1–38. https://doi.org/10.1080/05384680.1958.11904091

Wanninkhof R (2014) Relationship between wind speed and gas exchange over the ocean revisited. Limnology and Oceanography Methods 12: 351–362. https://doi.org/10.4319/lom.2014.12.351

Weiss RF (1974) Carbon dioxide in water and seawater: The solubility of a non-ideal gas. Marine Chemistry 2: 203–215. https://doi.org/10.1016/0304-4203(74)90015-2

Weiss RF, Price BA (1980) Nitrous oxide solubility in water and seawater. Marine chemistry 8: 347–359. https://doi.org/10.1016/0304-4203(80)90024-9

Williams JR, Giering SLC, Baker CA, Pabortsava K, Briggs N, East H, Espinola B, Blackbird S, Le Moigne FAC, Villa-Alfageme M, Poulton AJ, Carvalho F, Pebody C, Saw K, Moore CM, Henson SA, Sanders R, Martin AP (2025) Inefficient transfer of diatoms through the subpolar Southern Ocean twilight zone. Nature Geoscience 18: 72–77. https://doi.org/10.1038/s41561-024-01602-2

Wright SW, Ishikawa A, Marchant HJ, Davidson AT, van den Enden RL, Nash GV (2009) Composition and significance of picophytoplankton in Antarctic waters. Polar Biology 32: 797–808. https://doi.org/10.1007/s00300-009-0582-9

Yang Y, Gao K, Xue L (2016) Relationships between phytoplankton biomass and carbon flux in marine systems: A case study in coastal waters of China. Marine Pollution Bulletin, 113: 189–195.

Yin H, Jin L, Hu X (2024) Interpreting biogeochemical processes through the relationship between total alkalinity and dissolved inorganic carbon: Theoretical basis and limitations. Limnology and Oceanography: Methods 22: 311–320. https://doi.org/10.1002/lom3.10608

Zapata M, Rodríguez F, Garrido JL (2000) Separation of chlorophylls and carotenoids from marine phytoplankton: a new HPLC method using a reversed phase C8 column and pyridine-containing mobile phases. Marine Ecology Progress Series 195: 29–45. https://doi.org/10.3354/meps195029

Zeebe RE, Wolf-Gladrow D (2001) $CO_2$ in seawater: equilibrium, kinetics, isotopes. Elsevier, Amsterdam.

## FIGURES & FIGURE CAPTIONS

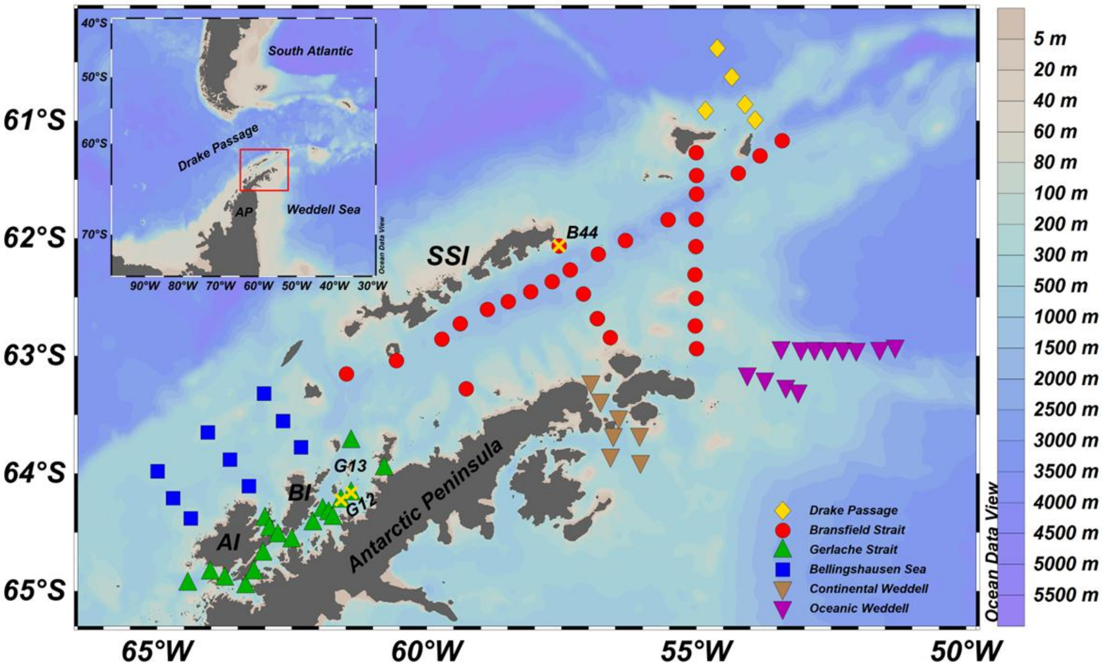

**Figure 1:** Study area and stations' locations during January 2019 along the Northern Antarctic Peninsula. Hydrographic stations in the Drake Passage (DP), Bransfield Strait (BS), Gerlache Strait (GS), Bellingshausen Sea (BL), Continental Weddell (CW), and Oceanic Weddell (OW) are represented by yellow diamonds, red circles, green triangles, blue squares, and brown and purple inverted triangles, respectively. The abbreviations are as follows: AI, Anvers Island; AP, Antarctic Peninsula; BI, Brabant Island; SSI, South Shetland Islands. The stations B44, G13, and G12 are highlighted with yellow 'x'. These stations were sampled more than once at weekly intervals, as shown in Figs. 6 and 7.

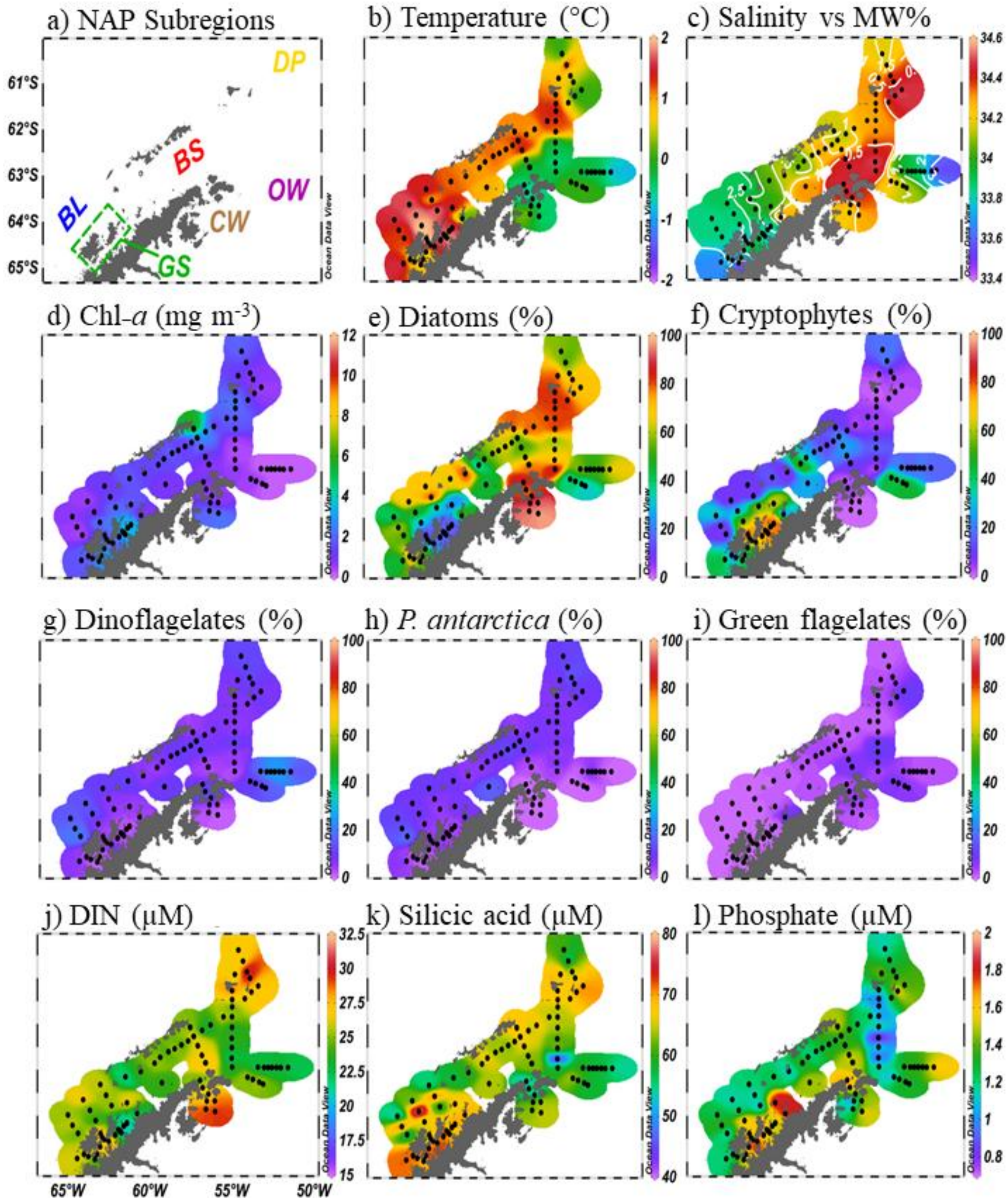

**Figure 2:** NAP Subregions, where Drake Passage (DP), Bransfield Strait (BS), Gerlache Strait (GS), Bellingshausen Sea (BL), Continental Weddell (CW) and Oceanic Weddell (OW) (**a**), surface distribution of temperature (**b**), salinity (colour scale) and meltwater percent (MW%; contour lines) (**c**), chl-*a* (mg m$^{-3}$) (**d**), relative diatom contribution (%) (**e**), relative cryptophyte contribution (%) (**f**), relative dinoflagellate contribution (%) (**g**), relative *P. antarctica* contribution (%) (**h**), relative green flagellates contribution (%) (**i**), DIN (**j**), Silicic acid (**k**), and Phosphate (**l**). Note the different scales. Black dots represent stations' location.

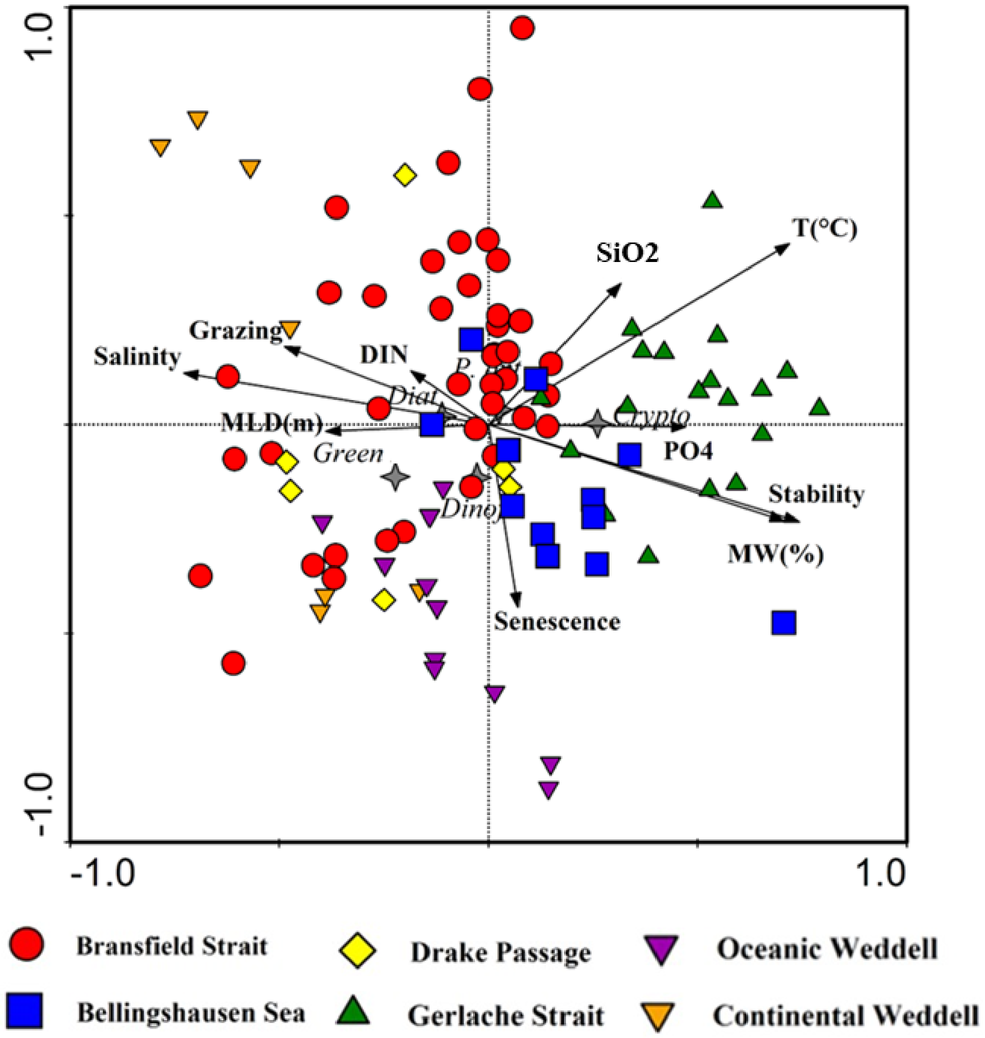

**Figure 3:** Canonical correspondence analysis (CCA) ordination diagram regarding to the relative contribution of phytoplankton groups. Arrows indicate explanatory variables: upper water column stability (Stability), temperature (T°C), meltwater percent (MW%), senescence and grazing indexes, salinity, mixed layer depth – MLD (m), DIN, phosphate ($PO_4$), and silicic acid ($SiO_2$). Grey crosses refer to relative contribution of phytoplankton groups. Crypto, cryptophytes; Diat, diatoms; Dino, dinoflagellates; P. ant, *Phaeocystis antarctica*; and Green, green flagellates.

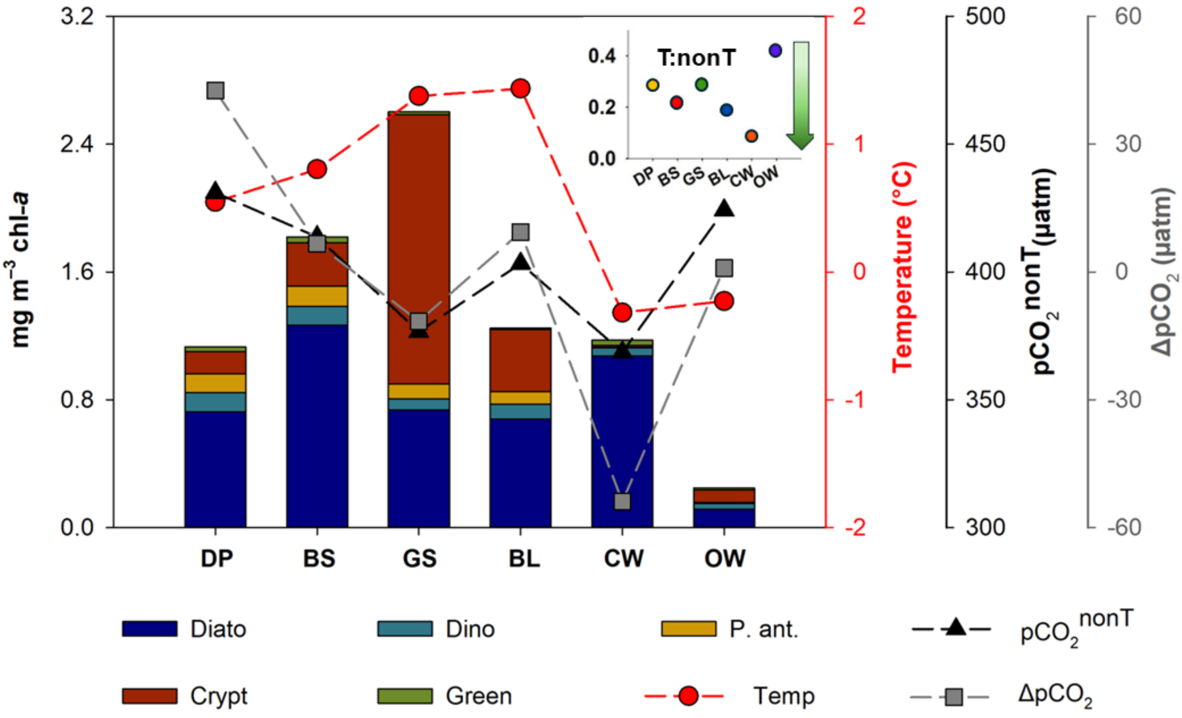

**Figure 4:** Average absolute contribution (mg m$^{-3}$ chl-*a*) of phytoplankton groups over the NAP subregions. Drake Passage, DP; Bransfield Strait, BS; Gerlache Strait, GS; Bellingshausen Sea, BL; Continental Weddell, CW; and Oceanic Weddell, OW. Averages of temperature (red circles), $pCO_2^{nonT}$ (black triangles), and $\Delta pCO_2$ (grey squares) are shown. The inset figure in the upper right corner shows values of T:nonT ratio for each subregion. Diato, diatoms; Dino, dinoflagellates; P. ant., *Phaeocystis antarctica*; Crypt, cryptophytes; Green, green flagellates; and Temp, temperature. See Supplementary Material Table S4 to confer the average, standard derivation, and the minimum and maximum values.

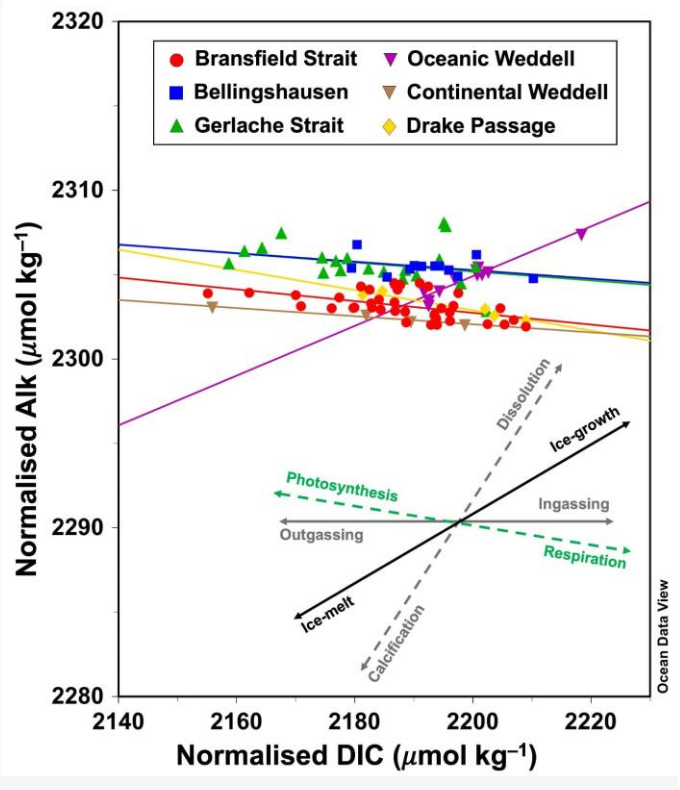

**Figure 5:** Normalised alkalinity (μmol kg$^{-1}$) and normalised dissolved inorganic carbon (DIC; μmol kg$^{-1}$) dispersion diagram. Subregions are represented by red dots (Bransfield Strait), blue squares (Bellingshausen), green triangles (Gerlache Strait), yellow diamond (Drake Passage), and brown (Continental Weddell) and purple (Oceanic Weddell) inverted triangles. The inset arrows show the potential drivers.

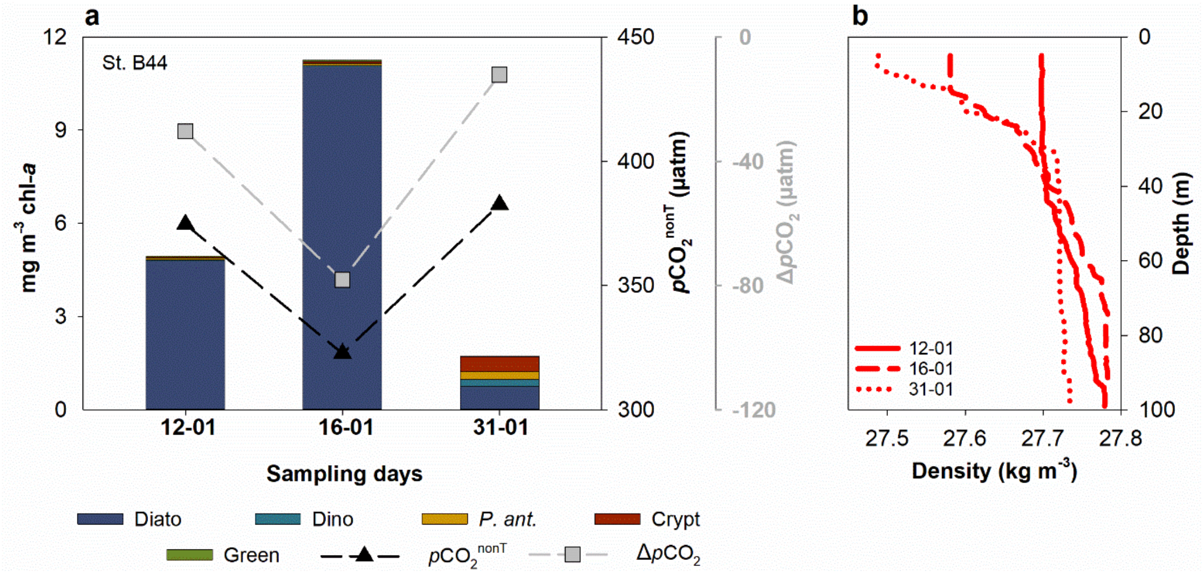

**Figure 6:** Station B44 sampled at weekly intervals in the Bransfield Strait in January 2019. **(a)** Absolute contribution (mg m$^{-3}$ of chl-*a*) of phytoplankton groups along with $pCO_2^{nonT}$ (pink triangles) and $\Delta pCO_2$ (grey squares). **(b)** vertical profile of water column density (kg m$^{-3}$). Diato, diatoms; Dino, dinoflagellates; P. ant., *Phaeocystis antarctica*; Crypt, cryptophytes; and Green, green flagellates.

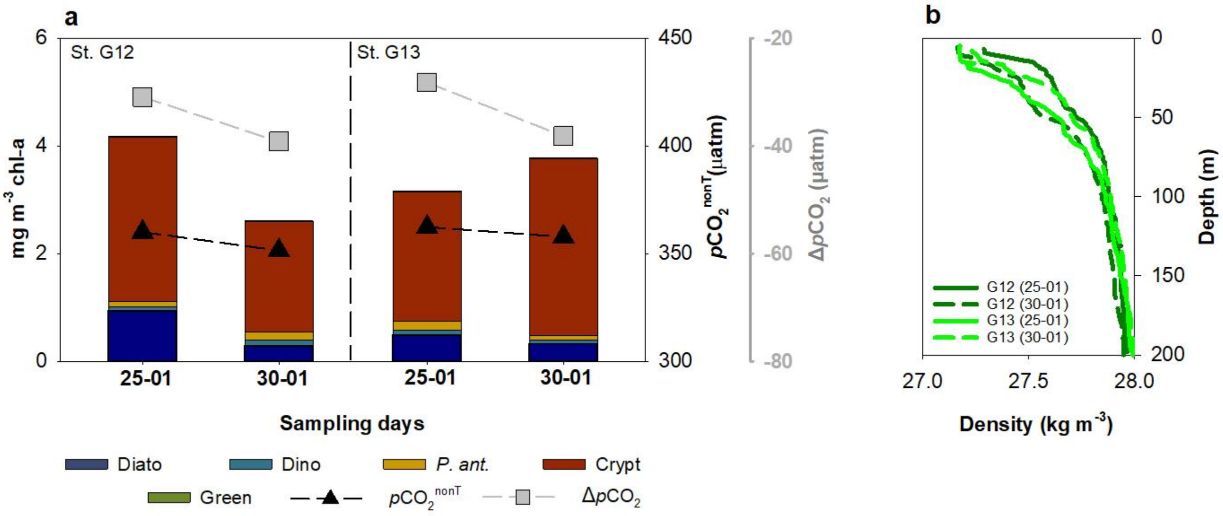

**Figure 7:** Stations G12 and G13 sampled at weekly interval in the Gerlache Strait in January 2019. **(a)** Absolute contribution (mg m$^{-3}$ of chl-*a*) of phytoplankton groups along with $p\mathrm{CO}_2^{\mathrm{nonT}}$ (pink triangles) and $\Delta p\mathrm{CO}_2$ (grey squares). **(b)** vertical profile of water column density (kg m$^{-3}$). Diato, diatoms; Dino, dinoflagellates; P. ant., *Phaeocystis antarctica*; Crypt, cryptophytes; and Green, green flagellates.